PHYSICAL REVIEW B VOLUME 20, NUMBER 12 15 DECEMBER 1979

Dynamic correlations in an electron gas. I. First-order perturbation theory

A. Holas,* P. K. Aravind, and K. S. Singwi
Department of Physics and Astronomy, Northwestern University, Evanston, Illinois 60201
(Received 29 May 1979)

Properties of a uniform electron gas in the jellium model are investigated by means of perturbation theory in the electron-electron interaction. First-order diagrams for the proper polarizability are evaluated for arbitrary wave vector and frequency, their singularities and analytical properties are examined, and a reliable numerical procedure for calculating them is established. Quantities such as the dielectric function $\epsilon(k,\omega)$, the dynamic-complex-local-field factor $G(k,\omega)$, dynamic structure factor $S(k,\omega)$, static structure factor $S(k)$, and pair correlation function $g(r)$ are calculated and compared with the corresponding quantities in the random-phase approximation (RPA). The plasmon dispersion in a wide range of momentum transfers and the shape of $S(k,\omega)$ versus ω agree well with experimental data for Al, indicating that the first-order theory is reasonable even at r_s as large as 2. Significant improvement over RPA is observed.

I. INTRODUCTION

Since the pioneering work of Bohm and Pines[1] and Lindhard,[2] done almost three decades ago, much effort has gone into developing a theory, which is valid for all wave vectors and frequencies, of the dielectric function of a homogeneous electron gas at metallic densities. The latter quantity plays an important role in determining many of the properties of metals. The simple theory of the dielectric function which goes under the name of random-phase approximation[3] (RPA) has been fairly successful in accounting for many metallic properties for the reason that it treats properly the long-range part of the Coulomb interaction. However, it neglects the important short-range exchange and correlation effects among the electrons and this causes the theory to display some undesirable features, e.g., negative values of the pair correlation function $g(r)$ at short distances.

In recent years several attempts[4-16] have been made to improve upon the RPA using different mathematical approaches and approximations. In the formulation of Singwi *et al.*,[5] it was argued that the exchange and correlation effects which lead to a local depletion in the density around each electron should be expressible in terms of the static pair correlation function. The latter is then determined self-consistently through the use of the fluctuation-dissipation theorem. A modified version of this theory due to Vashishta and Singwi,[15] which took care of the compressibility sum rule, has been fairly successful in its applications. In particular, it leads to very good results for the phonon dispersion relations[17] of simple metals. This is true of some other theories[12,14] too.

The various theories that have been proposed as improvements on the RPA include short-range exchange-correlation effects in an approximate way through a static-local-field factor $G(k)$. The assumption of a static local field implies that as a particle moves in response to a perturbing force it carries its exchange-correlation hole rigidly with it. This is true only if the perturbing force varies slowly in time as is the case, for example, in the calculation of phonon frequencies: Here the electrons respond instantaneously to the much slower motion of the ions and the exchange-correlation hole is able to adjust itself continuously to the motion of the particle it surrounds without distorting appreciably from its static value. For a rapidly varying external perturbation, the behavior of the exchange correlation hole is much more complicated: It deforms appreciably and also executes a dynamical motion relative to the particle as it attempts to keep up with it. Both these effects can be described adequately only by a complex, frequency-dependent local field $G(\vec{k},\omega)$. The complex nature of G follows very generally from causality arguments[18] and is necessary to include properly dissipative effects which give rise to a damping of the long wavelength plasmon.

For external fields characterized by frequencies much less than the plasma frequency ω_p, the inverse of which is a measure of the characteristic time of the medium, a static local field is a good approximation. On the other hand, for external fields varying with frequencies comparable to ω_p only a dynamic local field can provide an adequate description of the system response. It shall be our purpose in this paper to construct such a dynamical local field for the electron liquid. In the past there was not much incentive to include dynamic effects in the local field, but it has now become imperative to do so if we are to understand the results of recent inelastic electron[19-22] and x-ray[23] scattering experiments in simple metals.

 © 1979 The American Physical Society

Such experiments probe the excitation spectrum of density fluctuations in the system and thereby measure the dynamic structure factor $S(\vec{k},\omega)$, which in turn depends on the dynamic local field $G(\vec{k},\omega)$. Both the simple RPA and the mean-field theories of Singwi *et al.*[4,15] fail to reproduce the experimentally observed $S(\vec{k},\omega)$, particularly at large momentum transfers. As pointed out above, the failure of these theories to account adequately for the dynamical response of the system is due to their complete neglect of dynamical and dissipative effects in the local field (in the RPA, $G=0$ and in the theories of Singwi *et al.* it is purely real and static).

To formulate a microscopic approach to the problem of dynamical correlations which is physically transparent and at the same time tractable enough to yield results that can be compared with experiment is a far from easy task. The work of Brosens *et al.*[33] can be regarded as a first step in this direction. In a future publication[24] in this series of papers we shall make an attempt to develop a theory of dynamical correlations by starting from the exact quantum mechanical equations of motion for the system formulated in terms of the Wigner distribution functions. For the present, however, we shall content ourselves with a more straightforward attack on the problem which is based on the methods of perturbation theory. This paper should be viewed as exploratory in character, the aim being to see what one can learn about dynamical correlations in the electron liquid from a low-order perturbation calculation that can be done exactly.

In the above context, the quantity of basic interest is the screened response function or the irreducible polarization propagator $\pi(k,\omega)$. The lowest-order term in the perturbation series for π gives the RPA. In the next approximation one calculates the first-order diagrams, which consist of both self-energy and exchange contributions. This was done in the $\omega\to 0$ limit in an important paper by Geldart and Taylor,[13] who examined the consequences of these and some higher-order diagrams for the static screening function.[14] However, the full impact of these diagrams can be realized only by evaluating them for *arbitrary frequencies* and this is what we propose to do in this paper. We find that the first-order graphs display pathological singularities for some values of frequency. While this is not entirely unexpected, as foreshadowed earlier in the work of Glick,[31] the situation nevertheless demands detailed examination. By carefully examining the nature of the singularities encountered in our calculation, we are led to important conclusions about the validity of perturbation theory. Our main conclusion is that the perturbation theory for π is not valid for all frequencies (for a given $\vec{k}$) but breaks down in the neighborhood of the characteristic frequencies $\omega_s=\left|\frac{1}{2}k^2\pm k\right|$. This information will prove most helpful in interpreting the results of our future work.

The plan of this paper is as follows: In Sec. II, we introduce our notation and write down the expressions for the first-order diagrams. In Sec. III we examine the high-frequency properties of these diagrams, their connection with the frequency moment sum rules and the long wavelength plasmon dispersion. In Sec. IV, we present the final results of our evaluation of the first-order diagrams, relegating the details of the calculation to Appendices A and B. A comparison is made with the zeroth-order diagram (i.e., the Lindhard function) in order to estimate the relative importance of the correction we have calculated. A detailed examination of the singularities present in the theory is taken up in Sec. V and the structure of the perturbation theory is analyzed. Section VI contains a discussion of the dynamic local field $G(k,\omega)$ in this theory and we also comment upon the work of other authors.[33-35,39] In Sec. VII we present the results for $S(k,\omega)$, the plasmon dispersion, the static structure factor $S(k)$, and the pair correlation function $g(r)$. Finally, Sec. VIII contains our concluding remarks.

II. FIRST-ORDER DIAGRAMS FOR THE PROPER POLARIZABILITY

The diagrammatic expansion for the proper (or irreducible) polarization propagator $\pi(k)$ has been developed in many textbooks[25] and will not be rederived here. The lowest-order graphs for π are shown in Fig. 1. The zeroth-order contribution π^0 is, of course, just the Lindhard function:

$$\pi^0(k)=-\frac{2}{\hbar}\int\frac{d^4p}{(2\pi)^4 i}G^0(p)G^0(p+k)\,. \tag{2.1}$$

We shall use the 4-vector notation $k=(\vec{k},\omega)$, $p=(\vec{p},p_0)$, etc. The free-particle Green's function G^0 is given by

$$G^0(p)=\frac{1}{p_0-\omega_{\vec{p}}-i\eta\,\mathrm{sgn}(k_F-|\vec{p}|)},\quad \eta=0^+ \tag{2.2}$$

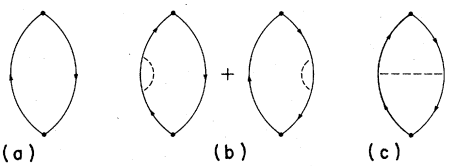

FIG. 1. Diagrams for proper polarizability: (a) the zeroth order, (b) and (c) the first-order self-energy and exchange contributions, respectively.

where k_F is the Fermi wave vector and $\omega_{\vec{p}} = \hbar\vec{p}^2/2m$. The first-order graphs divide into a self-energy part π^{SE} and an exchange part π^{Ex}. The expressions for π^{SE} and π^{Ex} are easily written down using the standard Feynman rules:

$$\pi^{SE}(k) = \frac{2}{\hbar}\int \frac{d^4p}{(2\pi)^4 i} G^0(p)G^0(p+k) \times[\Sigma^0(p)G^0(p) + \Sigma^0(p+k)G^0(p+k)], \tag{2.3}$$

$$\pi^{Ex}(k) = -\frac{2}{\hbar}\int \frac{d^4p}{(2\pi)^4 i}\frac{d^4p'}{(2\pi)^4 i} G^0(p)G^0(p+k) \times v(\vec{p}-\vec{p}')G^0(p')G^0(p'+k), \tag{2.4}$$

where

$$v(\vec{q}) = 4\pi e^2/\vec{q}^2, \tag{2.5}$$

and

$$\Sigma^0(p) = -\frac{1}{\hbar}\int \frac{d^4p'}{(2\pi)^4 i} v(\vec{p}'-\vec{p})G^0(p')\exp(ip_0'\eta) \tag{2.6}$$

is the Hartree-Fock self-energy.

The frequency integrals in (2.3) and (2.4) are easily performed by contour integration. Once this is done we can switch from the interaction representation to the more physically relevant retarded form[26] by shifting any poles lying above the real ω axis to below it. In this way we obtain

$$\pi^{SE}(\vec{k},\omega) = \frac{+2}{\hbar^2}\int \frac{d^3p}{(2\pi)^3}\int \frac{d^3p'}{(2\pi)^3} v(\vec{p}-\vec{p}')\frac{(n^0_{\vec{p}} - n^0_{\vec{p}+\vec{k}})(n^0_{\vec{p}'} - n^0_{\vec{p}'+\vec{k}})}{(\omega + \omega_{\vec{p}} - \omega_{\vec{p}+\vec{k}} + i\eta)^2}, \tag{2.7}$$

$$\pi^{Ex}(\vec{k},\omega) = -\frac{2}{\hbar^2}\int \frac{d^3p}{(2\pi)^3}\int \frac{d^3p'}{(2\pi)^3} v(\vec{p}-\vec{p}')\frac{(n^0_{\vec{p}} - n^0_{\vec{p}+\vec{k}})(n^0_{\vec{p}'} - n^0_{\vec{p}'+\vec{k}})}{(\omega + \omega_{\vec{p}} - \omega_{\vec{p}+\vec{k}} + i\eta)(\omega + \omega_{\vec{p}'} - \omega_{\vec{p}'+\vec{k}} + i\eta)}, \tag{2.8}$$

where $n^0_{\vec{p}} = \theta(k_F - |\vec{p}|)$ is the free-particle Fermi function at $T=0$. Before proceeding further it is convenient to express the integrals in dimensionless form. Introduce the dimensionless polarizabilities

$$Q^{SE,Ex}(\vec{k},\omega) = -v(\vec{k})\pi^{SE,Ex}(\vec{k},\omega), \tag{2.9}$$

and measure wave vectors in units of $k_F = 1/\alpha a_0 r_s$, $\alpha = (4/9\pi)^{1/3}$ and frequencies in units of $2E_F/\hbar$ ($E_F = \hbar^2 k_F^2/2m$ is the free Fermi energy). Equations (2.7) and (2.8) are then transformed to

$$Q^{SE,Ex}(\vec{k},\omega) = \frac{\alpha_D^2}{\vec{k}^2}F^{SE,Ex}(\vec{k},\omega), \tag{2.9a}$$

$$F^{SE}(\vec{k},\omega) = -\frac{1}{2}\int \frac{d^3p\,d^3p'}{(\vec{p}-\vec{p}')^2}\frac{(n^0_{\vec{p}} - n^0_{\vec{p}+\vec{k}})(n^0_{\vec{p}'} - n^0_{\vec{p}'+\vec{k}})}{(\omega + \omega_{\vec{p}} - \omega_{\vec{p}+\vec{k}} + i\eta)^2}, \tag{2.10}$$

$$F^{Ex}(\vec{k},\omega) = \frac{1}{2}\int \frac{d^3p\,d^3p'}{(\vec{p}-\vec{p}')^2}\frac{(n^0_{\vec{p}} - n^0_{\vec{p}+\vec{k}})(n^0_{\vec{p}'} - n^0_{\vec{p}'+\vec{k}})}{(\omega + \omega_{\vec{p}} - \omega_{\vec{p}+\vec{k}} + i\eta)(\omega + \omega_{\vec{p}'} - \omega_{\vec{p}'+\vec{k}} + i\eta)}. \tag{2.11}$$

In these formulas $\omega_{\vec{q}} = \frac{1}{2}\vec{q}^2$ and $\alpha_D = \alpha r_s/\pi^2$.

The functions F^{SE} and F^{Ex} are complex at finite ω but become purely real when $\omega = 0$. The first-order static polarizability is thus given by the real quantity

$$Q^1(\vec{k},0) = Q^{SE}(\vec{k},0) + Q^{Ex}(\vec{k},0) = \frac{\alpha_D^2}{\vec{k}^2}[F^{SE}(\vec{k},0) + F^{Ex}(\vec{k},0)]. \tag{2.12}$$

It is precisely the expression (2.12) that has been evaluated by Geldart and Taylor[13] [in their notation $F_{A,B}(k) = \alpha_D F^{Ex,SE}(\vec{k},0)$]. We shall here extend their $\omega = 0$ calculation to arbitrary frequencies.

We first consider the imaginary part of Q^1 which turns out to be simpler to evaluate than its real part. Leaving the details of the calculation to Appendices A and B, we present only the final results:

$$\mathrm{Im}F^{SE,Ex}(\vec{k},\omega) = \frac{4\pi^3}{k^2}[\theta(1-\nu_+^2)\Phi^{SE,Ex}(\nu_+,k) - \theta(1-\nu_-^2)\Phi^{SE,Ex}(\nu_-,k)], \tag{2.13}$$

where

$$\nu_\pm = \pm\frac{\omega}{k} - \frac{k}{2}, \quad k = |\vec{k}|,$$

$$\Phi^{SE}(\nu,k) = \nu f_L(\nu) - (\nu+k)f_L(\nu+k) + k f_L(((\nu+k)^2 + 1 - \nu^2)^{1/2}),$$

$$f_L(x) = \frac{1}{2} + \frac{1-x^2}{4x}\ln\left|\frac{1+x}{1-x}\right|.$$

It is noteworthy that $\mathrm{Im}F^{SE}$ can be evaluated analytically in closed form without recourse to numerical integration.

The expression for Φ^{Ex} is somewhat unwieldy:

$$\Phi^{Ex}(\nu,k) = -G_1(\nu) + G_2(\nu+k, 1-\nu^2), \tag{2.14}$$

where

$$G_1(\nu) = \tfrac{1}{4}(1-\nu^2)g\left(\frac{1-\nu}{1+\nu}\right) - \tfrac{1}{2}\nu[(1-\nu)\ln(1-\nu) + (1+\nu)\ln(1+\nu) - 2\ln 2], \tag{2.15}$$

with

$$g(a) = \begin{cases} \int_a^{1/a} \frac{dx}{x}\ln(1+x), & \text{if } 0 \le a \le 1 \\ -g(1/a), & \text{if } 1 \le a < \infty. \end{cases} \tag{2.16}$$

The θ functions in (2.13) ensure that $g(a)$ and all logarithms are only needed for positive arguments:

$$G_2(x_1,x_2) = -\tfrac{1}{4}\mathrm{P}\int_{-1}^{+1} d\xi \frac{T(\xi,x_1,x_2)}{\xi - x_1}. \tag{2.17}$$

To express T compactly we introduce the following auxiliary functions:

$$\gamma_0(x_1,x_2) = x_1^2 + x_2, \tag{2.18}$$

$$A_1(\xi,x_1) = 2(\xi - x_1)^2, \tag{2.19}$$

$$A_2(\xi,x_1) = 4(1-\xi^2)(\xi - x_1)^2, \tag{2.20}$$

$$A_3(\xi,x_1) = 2\xi(\xi - x_1) - 1, \tag{2.21}$$

$$t(\xi,x_1,x_2) = \frac{[(\gamma_0 + A_3)^2 + A_2]^{1/2} - (\gamma_3 + A_3)}{2(1-\xi^2)}. \tag{2.22}$$

In terms of these functions

$$T(\xi,x_1,x_2) = \left(\frac{A_1}{2t} - \frac{A_1}{2} + (1-\xi^2)(1-t)\right) \times \ln|A_1 + 2(1-\xi^2)t| - x_2 \ln A_1 + (1-\xi^2)[t - 1 - \ln(t)]. \tag{2.23}$$

In Eqs. (2.22) and (2.23) the arguments of the functions occuring on the right-hand side have been omitted for brevity and are the same as those occuring in the defining equations (2.18)–(2.21). Taking stock of the formulas for $\mathrm{Im}F^{Ex}$, we see that it has been reduced to the evaluation of two one-dimensional integrals $g(a)$ and $G_2(x_1,x_2)$. Both these integrals possess well-behaved integrands and their evaluation by numerical methods poses no essential problems. (For more details see Appendix B.)

Having calculated both Φ^{SE} and Φ^{Ex}, we can construct the total imaginary part of the first-order proper polarizability

$$\mathrm{Im}Q^1(\vec{k},\omega) = \frac{4\pi^3\alpha_D^2}{k^4}\{\theta(1-\nu_+^2)[\Phi^{SE}(\nu_+,k) + \Phi^{Ex}(\nu_+,k)] - \theta(1-\nu_-^2)[\Phi^{SE}(\nu_-,k) + \Phi^{Ex}(\nu_-,k)]\}. \tag{2.24}$$

It is worth pointing out that the above form of the first-order polarizability is analogous to the following form of the zeroth-order polarizability:

$$\mathrm{Im}Q^0(\vec{k},\omega) = \frac{\alpha r_s}{k^2}\left[\theta(1-\nu_+^2)\left(\frac{1-\nu_+^2}{k}\right) - \theta(1-\nu_-^2)\left(\frac{1-\nu_-^2}{k}\right)\right]. \tag{2.25}$$

The real part of Q^1 can now be obtained numerically through the dispersion relation

$$\mathrm{Re}Q^1(\vec{k},\omega) = -\frac{1}{\pi}\mathrm{P}\int_{-\infty}^{\infty}\frac{\mathrm{Im}Q^1(\vec{k},\omega')}{\omega - \omega'}d\omega' \tag{2.26}$$

which follows[27] from the fact that $Q^1(\vec{k},\omega)$ is analytic in the upper half of the complex ω plane and falls off at large ω as $1/\omega^4$ (this latter fact is demonstrated in the next section).

III. HIGH-FREQUENCY BEHAVIOR OF $Q^1(\vec{k},\omega)$; SUM RULES AND PLASMON DISPERSION

Before discussing the nature of Q^1 for arbitrary $\vec{k}$ and ω, we shall first examine its behavior in the limiting case of large frequencies (and finite $|\vec{k}|$) where it takes on a particularly simple form. Because of the θ functions in Eq. (2.13), $\mathrm{Im}Q^1$ vanishes in this limit and only $\mathrm{Re}Q^1$ survives. On expanding the denominators of F^{SE} in Eq. (2.10) and F^{Ex} in Eq. (2.11) in powers of $1/\omega$ we obtain after some algebra (PV denotes Pathak and Vashishta[28])

$$Q^1(\vec{k},\omega) = \frac{\omega_p^4}{\omega^4}G_{HF}^{PV}(k) + O\left(\frac{1}{\omega^6}\right). \tag{3.1}$$

In this formula $\omega_p = \alpha^2(3r_s)^{1/2}$ is the plasma frequency at zero wave vector (expressed in units of $2E_F/\hbar$) and

$$G_{HF}^{PV}(k) = -\tfrac{3}{4}\int_0^\infty dq' q'^2[S_{HF}(q') - 1] \times\left(\frac{5}{6} - \frac{q'^2}{2k^2} + \frac{(k^2 - q'^2)^2}{4k^3q'}\ln\left|\frac{k+q'}{k-q'}\right|\right), \tag{3.2}$$

where

$$S_{HF}(q) = \begin{cases} \frac{3q}{4} - \frac{q^3}{16}, & 0 \le q \le 2 \\ 1, & q \ge 2 \end{cases} \tag{3.3}$$

is the Hartree-Fock static structure factor. G_{HF}^{PV} can be evaluated analytically. The result is[45,40]

$$G_{HF}^{PV}(k) = -\frac{3}{16k^3}\left(\ln\left|\frac{k+2}{k-2}\right|\left(-\tfrac{32}{63} + \tfrac{24}{35}k^2 - \tfrac{2}{5}k^4 + \tfrac{1}{6}k^6\right) + \ln\left|\frac{(k+2)(k-2)}{k^2}\right|\left(\tfrac{2}{35}k^7 - \tfrac{1}{630}k^9\right)\right) - \frac{2}{21k^2} + \tfrac{38}{315} + \tfrac{71}{840}k^2 + \tfrac{1}{840}k^4. \tag{3.4}$$

It has the following limiting properties:

$$G_{\rm HF}^{\rm PV}(k)=\tfrac{3}{20}k^2+O(k^4),\ \text{for small } k, \tag{3.5}$$

$$G_{\rm HF}^{\rm PV}(k=2)=-\frac{1}{16\times 315}\times(3\times 2^8\ln 4-1427)+\tfrac{41}{240}=0.2427, \tag{3.6}$$

$$G_{\rm HF}^{\rm PV}(k)=\tfrac{1}{3}+O(1/k^2),\ \text{for large } k. \tag{3.7}$$

The density-density response function (or total polarization propagator) is given by

$$\chi(\vec{k},\omega)=-\frac{1}{v(\vec{k})}\frac{Q(\vec{k},\omega)}{1+Q(\vec{k},\omega)}\ . \tag{3.8}$$

In the present order of approximation it is

$$\chi^1(\vec{k},\omega)=-\frac{1}{v(\vec{k})}\frac{Q^0(\vec{k},\omega)+Q^1(\vec{k},\omega)}{1+Q^0(\vec{k},\omega)+Q^1(\vec{k},\omega)}\ . \tag{3.9}$$

Knowing (3.1) and using the well-known result for large ω

$$Q^0(\vec{k},\omega)=-\frac{\omega_p^2}{\omega^2}-\frac{\omega_p^2}{\omega^4}\left(\frac{3k^2}{5}+\frac{k^4}{4}\right)+O\left(\frac{1}{\omega^6}\right), \tag{3.10}$$

we can calculate the leading terms in the asymptotic expansion of $\chi^1(\vec{k}\omega)$. We find that

$$-v(k)\chi^1(\vec{k},\omega)=\frac{M_1^{(1)}}{\omega^2}+\frac{M_3^{(1)}}{\omega^4}+O\left(\frac{1}{\omega^6}\right), \tag{3.11}$$

where

$$M_1^{(1)}=-\omega_p^2 \tag{3.12}$$

and

$$M_3^{(1)}=-\omega_p^2[k^4/4+3k^2/5+\omega_p^2[1-G_{\rm HF}^{\rm PV}(k)]]\ . \tag{3.13}$$

On the other hand, it can be shown[28] that the exact density-density response function also possesses an asymptotic expansion of the form (3.11) but with the $M_i^{(1)}$ replaced by the following M_i:

$$M_1=v(k)\frac{1}{\pi}\int_{-\infty}^{\infty}d\omega'\omega'\,{\rm Im}\chi(\vec{k},\omega')=-3r_s\alpha^4\ , \tag{3.14}$$

and

$$M_3=v(k)\frac{1}{\pi}\int_{-\infty}^{\infty}d\omega'\omega'^3{\rm Im}\chi(\vec{k},\omega')=-\omega_p^2\left(\frac{k^4}{4}+\frac{\langle E_{\rm kin}\rangle}{E_F}k^2+\omega_p^2[1-G^{\rm PV}(k)]\right). \tag{3.15}$$

In (3.15) $\langle E_{\rm kin}\rangle$ is the average kinetic energy per particle in the *interacting* electron gas and $G^{\rm PV}(k)$ is defined exactly as in Eq. (3.2) for $G_{\rm HF}^{\rm PV}(k)$ except that the Hartree-Fock structure factor $S_{\rm HF}(q)$ occurring there is replaced by the true $S(q)$ for the system. Equations (3.14) and (3.15) are often referred to as the first and third frequency moment sum rules, respectively. On comparing them with Eqs. (3.12) and (3.13) we see that $M_1^{(1)}=M_1$, whereas $M_3^{(1)}\neq M_3$. Thus our present theory, which corresponds to retaining only the zeroth- and first-order contributions to the proper polarizability π, satisfies the first moment (or f-sum rule) exactly but fulfills the third moment sum rule only approximately. The latter discrepancy arises because, firstly, $\langle E_{\rm kin}\rangle$ in Eq. (3.15) has been replaced by its free-particle value of $\frac{3}{5}E_F$ and, secondly, $G^{\rm PV}(k)$ has been replaced by $G_{\rm HF}^{\rm PV}(k)$ i.e., its Hartree-Fock value. Both these deficiencies can be rectified only by including a suitable class of higher-order diagrams for π which contain potential effects that restore the third moment to its correct value. It is a challenging (and as yet unsolved) problem to identify these diagrams. In a later publication[24] we shall develop a microscopic theory which satisfies exactly both the first- and third-moment sum rules.

We shall now obtain an expression for the plasmon dispersion at long wavelengths. Since the plasmon frequency is given by the pole of the density-density response function [in the present approximation, by the pole of the right-hand side of Eq. (3.9)], we have to solve the equation

$$1+Q^0(\vec{k},\omega)+Q^1(\vec{k},\omega)=0\ . \tag{3.16}$$

In the limit $\vec{k}\to 0$ and $\omega\approx\omega_p$ the imaginary parts of both Q^0 and Q^1 are zero because of the θ functions in Eqs. (2.25) and (2.24). For the real parts we find that

$${\rm Re}Q^0(\vec{k},\omega)=-\frac{\omega_p^2}{\omega^2}\left(1+\frac{3k^2}{5\omega^2}\right)+O(k^4) \tag{3.17}$$

and

$${\rm Re}Q^1(\vec{k},\omega)=\frac{\omega_p^4}{\omega^4}\frac{3k^2}{20}+O(k^4)\ . \tag{3.18}$$

Note that these formulas also happen to be the $\vec{k}\to 0$ limits of the high-frequency expressions for Q^0 and Q^1 [Eqs. (3.10) and (3.1)] derived earlier. Equation (3.16) may now be solved to yield

$$\omega_{pl}(k)=\omega_p+\frac{3}{10\omega_p}(1-\tfrac{1}{4}\omega_p^2)k^2+O(k^4)\ . \tag{3.19}$$

Defining $\tilde{\alpha}$ through the relation

$$\omega_{pl}(k)=\omega_p+\tilde{\alpha}k^2+O(k^4)\ , \tag{3.20}$$

we see from Eq. (3.19) that in the present case

$$\tilde{\alpha}=\tilde{\alpha}_{\rm RPA}(1-\tfrac{1}{4}\omega_p^2)\ , \tag{3.21}$$

where $\tilde{\alpha}_{\rm RPA}=3/10\omega_p$ is the contribution predicted by the RPA alone. This result has been derived earlier by Du Bois[29] and by Nozières and Pines.[30] For $r_s=2.07$, $\omega_p=0.68$, Eq. (3.21) predicts that $\tilde{\alpha}=0.39$, which agrees well with the experimental value of 0.38 ± 0.02 quoted by Batson *et al*.[19] for

A1. Since $\mathrm{Im}Q^0$ and $\mathrm{Im}Q^1$ vanish in the $\vec{k}\to 0$ limit, the long wavelength plasmon is undamped in the present approximation.

IV. DISCUSSION OF Q^1 AND ITS COMPARISON WITH Q^0

In Fig. 2 the function $\mathrm{Im}F^{\mathrm{SE}}(\vec{k},\omega)$ has been sketched as a function of frequency for the three cases $k<2$, $k=2$, and $k>2$. In all the cases $\mathrm{Im}F^{\mathrm{SE}}$ is an odd function of frequency; this follows from general symmetry requirements. Restricting ourselves to positive frequencies, we see that for both $k<2$ and $k>2$ $\mathrm{Im}F^{\mathrm{SE}}$ has jump discontinuities (shown by circles in the figures) at the characteristic frequencies $\omega_s=\frac{1}{2}k^2+k$ and $\left|\frac{1}{2}k^2-k\right|$. For $k=2$, there is only a single jump discontinuity at $\omega_s=4$, the second one disappearing at $\omega=0$. The origin of these discontinuities lies in the sharp cutoffs imposed by the free Fermi functions n_k^0, combined with the squared energy denominator occurring in (2.10).

A careful examination of Eqs. (2.15) and (2.17) reveals that the frequency derivative of $\mathrm{Im}F^{\mathrm{Ex}}$ also possesses singularities at the characteristic frequencies ω_s. However, the function $\mathrm{Im}F^{\mathrm{Ex}}$ itself is continuous. Thus $\mathrm{Im}Q^1$, which is proportional to the sum of $\mathrm{Im}F^{\mathrm{SE}}$ and $\mathrm{Im}F^{\mathrm{Ex}}$, has its singularity structure determined by $\mathrm{Im}F^{\mathrm{SE}}$, i.e., it has jump discontinuities at the characteristic frequencies.

$\mathrm{Re}Q^1$ is determined from $\mathrm{Im}Q^1$ by Hilbert transformation and it is easily shown that the jump discontinuities in the latter at ω_s give rise to logarithmic singularities in $\mathrm{Re}Q^1$ at the same frequencies. One can go further and deduce that the sign of the singularity in $\mathrm{Re}Q^1$ is the same as the sign of the jump in $\mathrm{Im}Q^1$ at that point, while the strength of the singularity is determined by the magnitude of the jump. Thus, for example, for $k<2$ and $\omega=\frac{1}{2}k^2+k$, $\mathrm{Im}Q^1$ has a negative jump and therefore the logarithmic singularity in $\mathrm{Re}Q^1$ at this point will approach minus infinity.

It should be pointed out at this stage that there exist four independent checks on our calculations for Re and $\mathrm{Im}Q^1$: (1) and (2) by making a high-frequency ($\omega\to\infty$) expansion of the right-hand side of the dispersion relation (2.26) and comparing it with Eq. (3.1) we obtain the two identities

$$\int_0^\infty d\omega'\omega'\mathrm{Im}Q^1(\vec{k},\omega')=0\,, \tag{4.1}$$

$$\int_0^\infty d\omega'\omega'^3\mathrm{Im}Q^1(\vec{k},\omega')=-\frac{\pi}{2}\omega_p^4 G_{\mathrm{HF}}^{\mathrm{PV}}(k)\,. \tag{4.2}$$

These furnish us with two independent checks on our calculations for $\mathrm{Im}Q^1$. To verify (4.1) we calculated the integral on the left-hand side and compared it with the integral of the absolute value of the same integrand. We found that the former in-

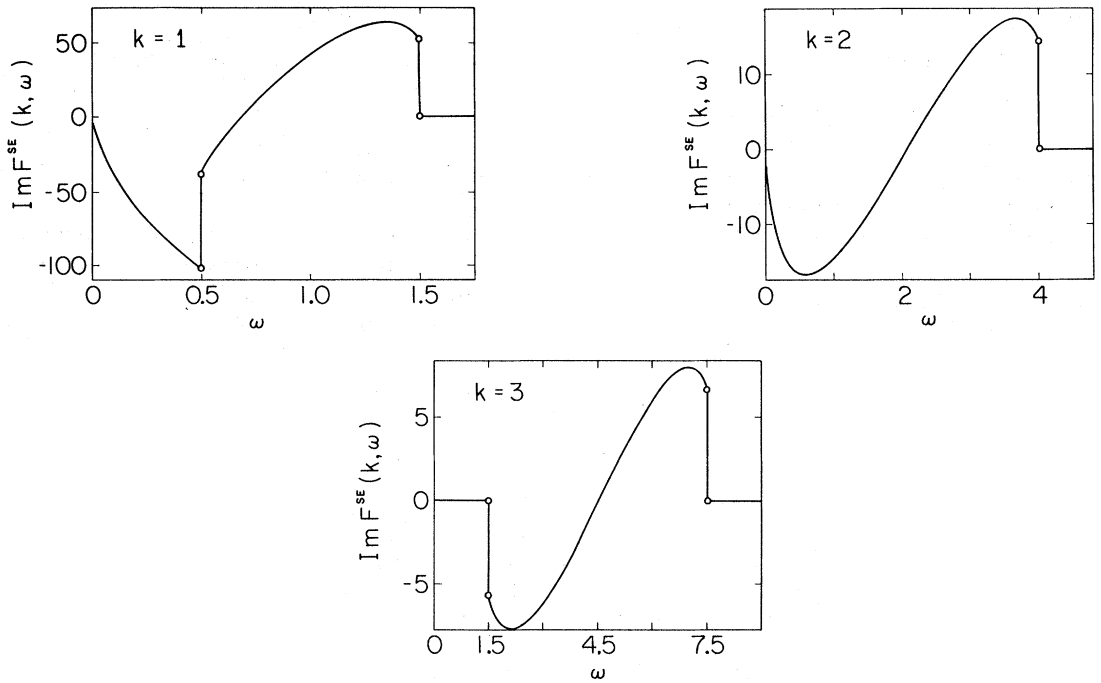

FIG. 2. Imaginary part of the self-energy contribution to proper polarizability. Its discontinuities at $\omega_s=|\frac{1}{2}k^2\pm k|$ are indicated by circles. Wave number k is expressed in units of k_F, frequency ω in $2E_F/\hbar$, here and on all other figures.

tegral was less than 10^{-5} times the latter, which can be regarded as an excellent numerical check of the identity (4.1). Regarding (4.2), it was found that the integral on the left-hand side agreed with the value of the right-hand side calculated through (3.4) to within 1 part in 10^4. (3) Our method of calculating Re and ImQ^1 is valid for all frequencies. On applying it to the case $\omega = 0$ we were able to make contact with the work of Geldart and Taylor.[13] We found that our calculated values of Re$Q^1(\vec{k},0)$ differed by less than 0.3% from the values quoted by these authors. Further, the agreement was found to become consistently better as we increased the fineness of the mesh involved in our numerical integration. (4) The last check also concerns the quantity Re$Q^1(\vec{k},0)$. Its values for large k (eg., $k=5$ and 10) were found to agree extremely well with the two-term asymptotic formula derived by Geldart and Taylor.[14] All these checks, taken together, provide us with valuable confirmation of the overall correctness of the analytical derivation and numerical procedure leading to the final results for Re and ImQ^1.

We will now discuss the r_s (density) dependence of the various graphs in the perturbation series for the dimensionless proper polarizability Q. We note that Q^n, which is the sum of all irreducible polarization graphs containing n interaction lines, behaves like

$$Q^n \sim k_F^{-(n+1)} \sim r_s^{n+1}. \tag{4.3}$$

In order to see this we enumerate all factors contributing to a typical graph: (1) $\sim k_F^{-2n}$ from n interaction potentials $4\pi e^2/q^2$, (2) $\sim E_F{}^{-2(n+1)} \sim k_F{}^{-4(n+1)}$ from $2(n+1)$ free-particle Green's functions $G^0 \sim 1/E_F$, (3) $\sim (E_F k_F^3)^{n+1} \sim k_F^{5(n+1)}$ from integration over $n+1$ intermediate 4-momenta, (4) $\sim k_F^{-2}$ from the factor $v(k)$ included in Q^n to make it dimensionless. The product of all these factors yields (4.3). Although the nth-order proper polarizability Q^n is seen to have a simple power dependence on r_s, the total Q does not simply form a power series in r_s.

The reason for this is the following. Some diagrams contributing to Q^n, $n \geq 2$, which contain polarization insertions, are divergent (e.g., second-order diagrams obtained from those in Figs. 1(b) and 1(c) by replacement of the dashed line by the dashed-bubble-dashed line. Nevertheless, the sum of an infinite number of such diagrams, equivalent to replacement of V_q by $V_q/\epsilon(q,\omega)$, in finite. The same difficulties (and for the same reason) are known in the case of the perturbation theory for the correlation energy. By analyzing the series for Q in the small r_s limit in a manner analogous to the correlation energy, as done by Gell-Mann and Bruckner,[32,3] one can establish that Q has the form of ln r_s times a power series in r_s plus another power series in r_s. In particular, the estimation

$$Q^2 + Q^3 + \cdots \sim O(r_s^3 \ln r_s,\ r_s^3) \tag{4.4}$$

justifies our neglect of these terms at high densities. In addition, it should be mentioned here that the perturbation expansion for $Q(k,\omega)$ may be invalid at some particular arguments (k,ω) (see Sec. V) for reasons unconnected with the infrared divergence of the Coulomb potential.

An examination of Fig. 3 gives a feeling for the relative magnitudes of the first-order polarizability Q^1 and the zeroth-order Q^0. All curves are plotted at $r_s = 2$ (which corresponds to the case of

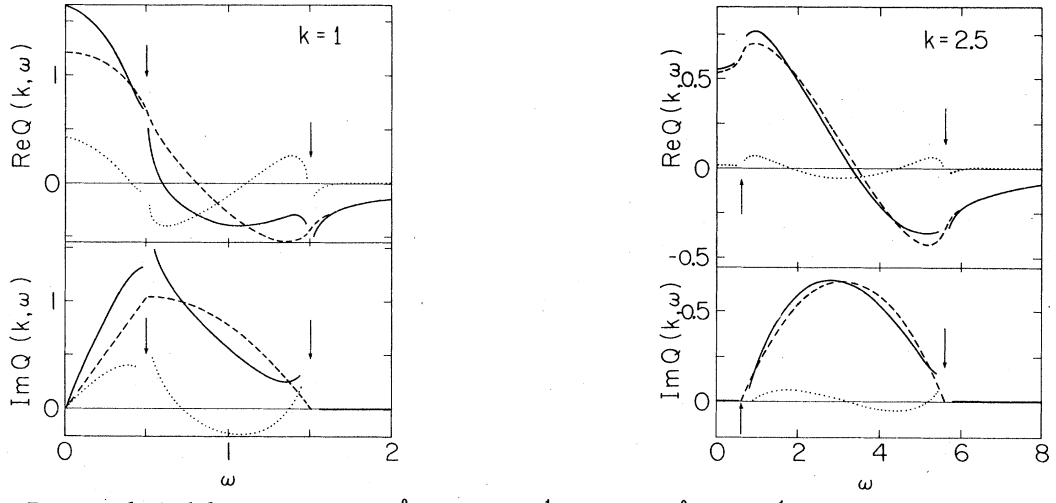

FIG. 3. Proper polarizability at $r_s = 2$. $---Q^0(k,\omega)$, $\cdots Q^1(k,\omega)$, $——Q^0(k,\omega)+Q^1(k,\omega)$. Arrows point out characteristic frequencies ω_s.

Al), but the simple relation (4.3) provides an easy way of rescaling the figure to a different r_s: Values of Q^0 should be multiplied by $r_s/2$, values of Q^1 by $(r_s/2)^2$. At $k=2.5$ typical values of Q^1 are approximately 10–15% of the typical values of Q^0 (both in real and imaginary parts). But for smaller k, e.g., $k=1$, the percentage increases to the range of 25–30%. This is a general tendency found for a series of k. We can conclude therefore that the approximation of Q by Q^0+Q^1 can be reasonable even at $r_s=2$, for larger k. For $k=1$ and smaller, the contribution from higher-order terms may become significant. Of course, when this approximation is applied at smaller r_s, the situation is always improved.

Regions close to characteristic frequencies ω_s, marked by arrows, are deliberately omitted on the figure for the reason explained in the following section.

We notice that Fig. 3 also gives, directly, information about the dynamic dielectric function $\epsilon(k,\omega)$, because it is defined as

$$\epsilon(k,\omega)=1+Q(k,\omega)\,. \tag{4.5}$$

V. SINGULARITIES OF THE FIRST-ORDER DIAGRAMS AND THEIR REMOVAL

The jump discontinuities in $\mathrm{Im}F^{\mathrm{SE}}$ and logarithmic singularities in $\mathrm{Re}F^{\mathrm{SE}}$ at $|\omega_s|=|\frac{1}{2}k^2\pm k|$, presented in the previous section, may lead to unphysical results for various quantities in the neighborhood of $|\omega_s|$. For example, the dielectric function $\epsilon(\vec{k},\omega)$ may have infinities and $S(\vec{k},\omega)$ may have zeros or even negative portions near $|\omega_s|$. These difficulties demonstrate that perturbation theory is not adequate for all frequencies. Any attempt at removing the singularities by the inclusion of higher-order perturbative effects leads to unmanageable complications. One is, therefore, forced to seek a simpler solution. In what follows we shall show that our approximation to Q is a reasonable one almost everywhere except in narrow ranges of frequency about the characteristic frequencies.

It was mentioned in Sec. IV that the squared denominator in expression (2.10) for F^{SE} caused $\mathrm{Im}F^{\mathrm{SE}}$ to be discontinuous at ω_s. On the other hand, the similar expression (2.11) for F^{Ex} involved the product of two different denominators and $\mathrm{Im}F^{\mathrm{Ex}}$ was found to be perfectly continuous everywhere. In terms of the diagrammatic representation, the presence of two Green's functions with the same arguments [as in π^{SE}, Eq. (2.3), Fig. 1(b)] is the source of the trouble. Higher-order diagrams which contain repeated Green's functions, such as those shown in Fig. 4, will also display the same pathological features as F^{SE}. We

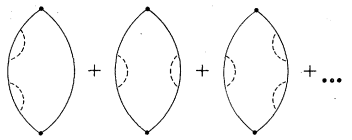

FIG. 4. Some second- and third-order polarizability diagrams involving self-energy insertions.

wish to consider the class of all diagrams of the type shown in Fig. 4, with π^0 and π^{SE} included for completeness. This general class, denoted by $\pi^{0,\mathrm{ef}}$, is represented by the basic bubble of Fig. 1(a), but with the free-particle Green's function G^0 replaced by the effective Green's function G^{ef} defined through the Dyson equation (see Fig. 5):

$$G^{\mathrm{ef}}(p)=G^0(p)+G^0(p)\,\Sigma^0(p)G^{\mathrm{ef}}(p)\,, \tag{5.1}$$

where $\Sigma^0(p)$ [see Eq. (2.6)] is the Hartree-Fock self-energy insertion. Equation (5.1) can be solved for G^{ef} to yield

$$G^{\mathrm{ef}}(p)=G^0(p)/[1-\Sigma^0(p)G^0(p)]\,. \tag{5.2}$$

In terms of G^{ef}, $\pi^{0,\mathrm{ef}}$ is given by

$$\pi^{0,\mathrm{ef}}(k)=-\frac{2}{\hbar}\int\frac{d^4p}{(2\pi)^4 i}G^{\mathrm{ef}}(p)G^{\mathrm{ef}}(p+k)\,. \tag{5.3}$$

Thus we see that all the troublesome diagrams, when summed up, give rise to a regular expression (5.3) containing no repeated Green's functions.

By making a formal expansion of the denominator of G^{ef}(5.2) in powers of the interaction [$\Sigma^0(p)\sim v$, see (2.6)] we easily recover the lowest-order diagrams:

$$\pi^{0,\mathrm{ef}}(k)=\pi^0(k)+\pi^{\mathrm{SE}}(k)+O(v^2)\,. \tag{5.4}$$

However, the expansion (5.4) does not converge to the full expression (5.3) at $\omega=\omega_s$ or converges very slowly in the neighborhood of ω_s. This means that at these particular frequencies the first-order diagram Q^1 cannot be separated out of the sum $(Q^1+Q^2+\cdots)$, which makes the first-order theory invalid there. (This effect can also further complicate the r_s dependence of Q at $\omega\approx\omega_s$, in addition to the logarithmic behavior discussed in Sec. IV.)

We can illustrate the foregoing remarks by means of a simplified but analytically tractable model, the so called effective mass approximation. Using

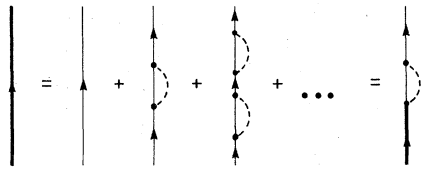

FIG. 5. Dyson's equation for effective Green's function $G^{0,\mathrm{ef}}$.

the definition of G^0, Eq. (2.2), the effective Green's function (5.2) becomes

$$G^{\mathrm{ef}}(p)=\frac{1}{p_0-\omega_p^*-i\eta\,\mathrm{sgn}(k_f-|\vec{p}|)}\,, \tag{5.5}$$

where

$$\omega_p^*=\omega_{\vec{p}}+\Sigma^0(p)\,. \tag{5.6}$$

The HF self-energy Σ^0 can be calculated explicitly and expressed in terms of a real and frequency-independent function $f_L(|\vec{p}|)$ [see Appendix A, Eq. (A4)] as

$$\Sigma^0(p)=\Sigma^0(|\vec{p}|)=-\frac{2\alpha r_s}{\pi}f_L(|\vec{p}|)\,. \tag{5.7}$$

In (5.7) Σ^0 has been expressed in units of $2E_F/\hbar$ and $|\vec{p}|$ in units of k_F. In the limit of small $\vec{p}$, Eq. (5.6) becomes

$$\omega_p^*=\omega_{\vec{p}}^*=\mathrm{const}+\tfrac{1}{2}\frac{m}{m^*}\vec{p}^{\,2}+O(|\vec{p}|^4)\,, \tag{5.8}$$

where

$$\frac{m}{m^*}=1+\frac{4\alpha r_s}{3\pi}\,. \tag{5.9}$$

In the effective mass approximation all terms in (5.8) higher than quadratic in the momentum are neglected (the constant term drops out later when the integration over frequencies is performed). Within this approximation, the right-hand side of (5.3) can be calculated analytically and one obtains

$$\pi^{0,\mathrm{ef}}(\vec{k},\omega)+\frac{m}{m^*}\pi^0\left(\vec{k},\frac{m^*}{m}\omega\right)\,, \tag{5.10}$$

which is simply a rescaled form of the Lindhard function.

Figure 6 shows the results of our calculations at $r_s=0.5$ and $k=0.5$, illustrating the problem under discussion. The full line represents the function $(Q^{0,\mathrm{ef}}-Q^0)$, which, according to (5.4), contains Q^{SE} plus all higher-order diagrams of the type shown in Fig. 4. As expected, the imaginary part of this function is continuous and the real part is finite. The broken line corresponds to the Q^{SE} contribution alone, which is discontinuous in its imaginary part and infinite in its real part. Both curves were calculated in the effective mass approximation. In order to test the goodness of the effective mass approximation we have also plotted the exact Q^{SE}, i.e., calculated with the true self-energy (5.7), by a dotted line in the figure. A comparison of the dotted and broken lines shows that while the effective mass approximation is not too accurate it is certainly good enough for our illustrative purposes. Returning to the functions $Q^{0,\mathrm{ef}}-Q^0$ and Q^{SE} (the full and broken lines in the figure), we see that the agreement between them

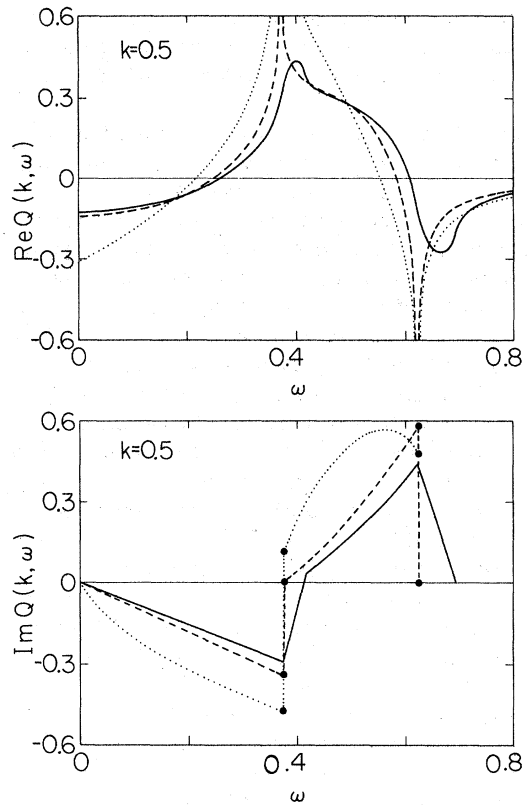

FIG. 6. Proper polarizability involving self-energy insertions at $r_s=0.5$. —— $Q^{0,\mathrm{ef}}-Q^0$, --- Q^{SE}—both curves within effective mass approximation, Eq. (5.8), $\cdots$ Q^{SE} with the true self-energy; Eqs. (2.3), (2.6).

is rather fair at all frequencies except in two narrow regions of width

$$\Delta\omega_s\cong 2\left(\frac{m}{m^*}-1\right)\omega_s \tag{5.11}$$

about the characteristic frequencies $\omega_s=\left|\tfrac{1}{2}k^2\pm k\right|$, where the discrepancy suddenly becomes extremely pronounced. Thus we find, in the effective mass approximation, that $Q^{0,\mathrm{ef}}$ can be approximated fairly well by Q^0+Q^{SE} (to within small perturbative corrections arising from second- and higher-order diagrams) for all frequencies except those in the neighborhood of ω_s.

It should be mentioned that in the small $\vec{k}$ limit Q^{SE} becomes even more singular than discussed above due to the merging together of the characteristic frequencies $\left|\tfrac{1}{2}k^2\pm k\right|$. This case has been investigated in detail by Glick.[31] In order to remove the very pathological singularities that are present here he found it necessary to use a screened Coulomb interaction (thereby eliminating the infrared divergence of the bare potential) and sum an infinite set of both bubble and ladder diagrams utilizing the renormalized Green's function

(5.2). Our calculation, which is a finite $\vec{k}$ version of Glick's, is much simpler to carry out because the singularities are far milder than in Glick's case.

The method we have described above for eliminating the singularities present in Q^{SE} suffers from two shortcomings: (i) It is carried out in the framework of the effective mass approximation, shown to be rather rough, and (ii) only diagrams of the type shown in Fig. 4 have been summed up. In actual practice one knows that there are large cancellations among diagrams of the same order and so it is absolutely necessary to retain *all* diagrams in each order to obtain consistent results. We shall not attempt to rectify these deficiencies since we would then be faced with the impossible problem of summing exactly the entire series for π. However, the main aim of our discussion has been not to eliminate the singularities, but rather to determine the region of validity of perturbation theory and this has been clearly established: We know that the first-order perturbation theory (for the present problem) is good at all frequencies except at those close to ω_s. Therefore we shall remain with our present approximation for Q ($\cong Q^0 + Q^{SE} + Q^{Ex}$) and merely exclude from consideration the dangerous frequency regions around ω_s where we know the theory becomes invalid.

VI. THE DYNAMIC LOCAL FIELD $G(\vec{k},\omega)$

Hitherto, the quantity of basic interest has been the proper polarizability π and we have evaluated it explicitly to first order in the potential v. We shall now focus our attention on the dynamic local field $G(\vec{k},\omega)$ which is defined formally through the relation

$$\chi(\vec{k},\omega) = -\frac{1}{v(\vec{k})}\frac{Q^0(\vec{k},\omega)}{1+Q^0(\vec{k},\omega)[1-G(\vec{k},\omega)]}\,. \tag{6.1}$$

On comparing Eqs. (6.1) and (3.8) we find that

$$G(k,\omega) = \frac{1}{Q^0(\vec{k},\omega)} - \frac{1}{Q(\vec{k},\omega)}\,, \tag{6.2}$$

where $Q = \sum_{n=0}^{\infty} Q^n$ is the dimensionless full proper polarizability. Since in the present (pr) case $Q \cong Q^0 + Q^1$, the local field becomes

$$G^{pr} = \frac{1}{Q^0} - \frac{1}{Q^0+Q^1} = \frac{Q^1}{Q^0(Q^0+Q^1)}\,. \tag{6.3}$$

In Eq. (6.3), and also subsequently, the arguments of functions will often be omitted for brevity.

The right-hand side of Eq. (6.2) can be recast in the form of a series in which successive terms involve increasing powers of the potential v. To do this it is necessary to assume that

$$\left|\frac{Q^1+Q^2+\cdots}{Q^0}\right| < 1 \tag{6.4}$$

(the vertical bars indicate the modulus of the complex quantity within it). The right-hand side of (6.2) can then be expanded out in a power series and the terms regrouped to yield

$$G = G^1 + G^2 + \cdots\,, \tag{6.5}$$

where

$$G^1 = \frac{Q^1}{(Q^0)^2}\,, \tag{6.6}$$

and

$$G^2 = \frac{Q^2}{(Q^0)^2} - \frac{(Q^1)^2}{(Q^0)^3} \tag{6.7}$$

are the terms of first and second order in v, respectively.

The series (6.5) for G has been derived by Dharma-wardana[34] by a very general method which does not make use of the condition (6.4). In Dharma-wardana's approach the quantity of interest is the mass operator $M(\vec{k},\omega)$ which is related simply to the local field by

$$M(\vec{k},\omega) = v(k)[1-G(\vec{k},\omega)]\,. \tag{6.8}$$

Using a Green's function formalism and developing a perturbation theory for the mass operator he obtains, to lowest order,

$$M^1 = v[1 - Q^1/(Q^0)^2]\,. \tag{6.9}$$

This is seen, via (6.8), to be equivalent to our G^1 (6.6). An expression is also obtained for M^2 which corresponds to our G^2(6.7). However, no attempt has been made to evaluate M^1 or M^2 explicitly and therefore the results of this work are somewhat inconclusive. (In the light of the discussion presented in Sec. IV, expansion (6.5) is rather formal; actually G^2 as well as M^2 cannot be separated from the sum with higher order terms, or, equivalently, M^2 and G^2 should represent infinite sums of subsets of diagrams, producing screening of the Coulomb interactions in the leading term.)

Two other groups of authors have also obtained Eq. (6.6) as the form of their total local field, but by following methods quite different from the one outlined above. We shall comment here briefly on their work:

(i) Brosens *et al.*[33] perform an exchange decoupling of the equations of motion to obtain an integral equation for the one-particle Wigner function. On solving this equation approximately by a variational method they are led to the expression (6.6) for their local field, which is therefore equivalent to the first-order approximation to the exact G (6.5) or exact M (6.8). Although in a subsequent

paper[46] these authors realize that their G is related to the perturbational result of Geldart and Taylor[13] (in the static limit), this did not prevent them from considering their approach to be applicable in the whole range of metallic densities. From our point of view, it is valid only as long as the effects of $G^2+\cdots$ are negligible, which seems to be questionable at $r_s=3$, the density for which they presented results. The values of the function $Q^1(\vec{k},\omega)$ obtained by these authors were found to agree well with our calculations. While the presence of singularities in Q^1 is noted, their role in $G(\vec{k},0)$, $S(\vec{k},\omega)$, and the plasmon dispersion is considered significant rather than unphysical, as we have shown in the previous section.

(ii) By writing the equations of motion for the Green's functions, accounting for the effects of potential to first order only, and using a decoupling procedure, Tripathi and Mandal[35] are also led to a local field of the form (6.6). These authors evaluate it only in the static limit and find that it has a sharp peak for k in the neighborhood of 2 (see Fig. 7, dash-dot line). In the light of our discussion in the previous section we know that this is a spurious effect since $\omega=0$, $k\simeq 2$ is a point at which the perturbation theory breaks down. In later publications[36,37,39,41] these authors go on to calculate the pair correlation function and various other static properties in terms of $G(\vec{k},0)$. Because integration over frequencies is involved, this procedure is justified only if $G(\vec{k},\omega)$ is approximated well for all frequencies by its static part and we shall see later that this is definitely not the case. Also, their claim that their theory conserves frequency moments to infinite order does not appear valid in general, because all terms higher than linear in potential are omitted. Their claim merely amounts to the statement that the frequency dependence is fully accounted for in the first-order term.

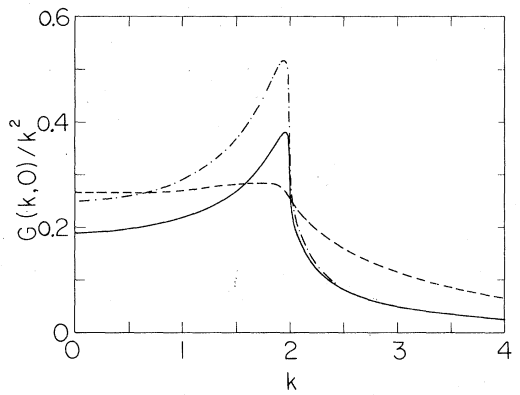

FIG. 7. Static part of the local field function $G(k,0)/k^2$: —— G^{pr}, Eq. (6.3), at $r_s=1.894$; --- G^1, Eq. (6.6); -·-·- G^{GT}, Ref. 14, at $r_s=1.894$.

We shall now show detailed results for the dynamic local fields G^{pr} and G^1. G^{pr}, Eq. (6.3), was obtained by retaining first-order terms (in v) in the perturbation expansion for the proper polarizability $Q\cong Q^0+Q^1$ and then using the general relation (6.2). On the other hand, G^1 was obtained by directly formulating a perturbation expansion for M or for G, Eq. (6.5), and keeping only the first-order term for them. Both G^{pr} and G^1 involve only the low-order polarizabilities Q^0 and Q^1 but are constructed out of them in different ways. While G^{pr} depends on r_s, the structure of G^1 makes it r_s independent. It is not clear *a priori* which of these forms is superior [i.e., leads to a better approximation to $G(\vec{k},\omega)$, $\chi(\vec{k},\omega)$, $S(\vec{k},\omega)$, etc.] and we will therefore show results for both of them, referring to the future to each type of approximation as $G^{pr}A$ and G^1A, respectively. Concerning the properties already discussed in Sec. III in $G^{pr}A$, we briefly summarize them in G^1A. High-frequency expansion of $\chi(k,\omega)$ in G^1A is exactly the same as (3.11) [the difference is $O(1/\omega^6)$]. Therefore G^1A theory satisfies the first moment exactly and third moment approximately,[40] with the same accuracy as $G^{pr}A$ theory. Long wavelength plasmon in G^1A has the same dispersion[33] as in $G^{pr}A$, Eq. (3.20); the difference is $O(k^4)$.

In Fig. 7 we show the static ($\omega=0$) parts of G^{pr} (continuous line) and G^1 (dot-dash line), divided by k^2, as a function of wave vector k. We also show a static local field due to Geldart and Taylor,[14] G^{GT}, which was obtained by including certain higher-order correlation diagrams in addition to the first-order diagrams and by using some renormalizations in order to obtain agreement with the compressibility sum rule. Both G^{pr} and G^{GT} were calculated at $r_s=1.894$. On examining Fig. 7 we see that both G^{pr} and G^1 exhibit a peaked structure around $k=2$, which is absent in G^{GT}, thereby indicating that this feature is an artifact of first-order perturbation theory and is washed out by higher-order correlation effects (this is in agreement with our general view of the perturbation expansion close to ω_s, as was pointed out earlier in this section[38]). By comparison of G^{pr}/k^2 and G^1/k^2 at $k\to 0$ with the limiting value of G^{GT}/k^2 which is so constructed that it gives the proper value of the compressibility of the electron gas, we can conclude that G^1 is more consistent than G^{pr} with the compressibility sum rule, though the magnitude of their difference is of the second order in potential only. At large k, G^{pr} and G^1 becomes practically identical and lie lower than G^{GT}.

In Fig. 8 we show the real and imaginary parts of G^{pr} and G^1 plotted as functions of frequency. The

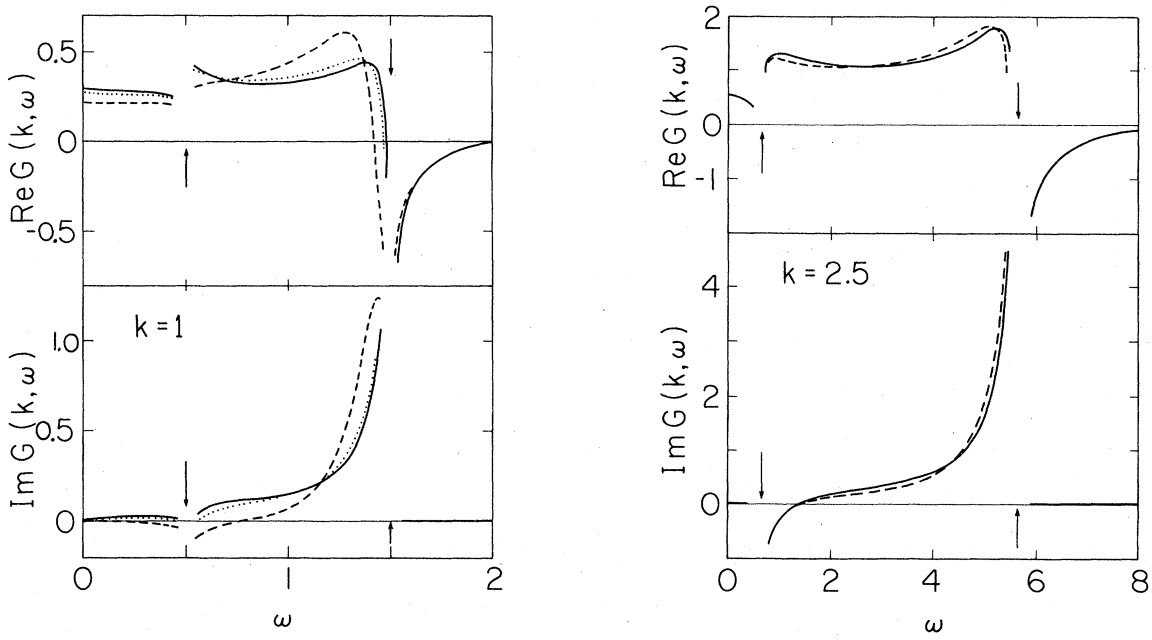

FIG. 8. Dynamic local field $G(k,\omega)$: —G^1, ····G^{pr} at $r_s=0.5$, ---G^{pr} at $r_s=2.0$.

three curves shown correspond to G^{pr} for the two r_s values 0.5 (dotted line) and 2.0 (dashed line), and G^1 (continuous line). [Note from (6.3) that $G^1=\lim r_s\to 0\ G^{pr}$]. The arrows show the positions of the characteristic frequencies ω_s where, in accordance with the discussion of the previous section, the curves cannot be trusted and for this reason these portions have been deliberately left incomplete. We see that G^1 and G^{pr} for $r_s=0.5$ agree closely at all frequencies for $k=1$ and are so close for $k=2.5$ that they could not be drawn separately. Function G^{pr} for $r_s=2.0$ differs somewhat from the two previous curves in the region below and between the frequencies ω_s, and agrees closely at large frequencies. We see that both $\mathrm{Re}G^1$ and $\mathrm{Re}G^{pr}$ rise from their static ($\omega=0$) values to a maximum located slightly below the upper characteristic frequency ω_s. Thereafter they seem to drop sharply and become negative before finally approaching the (positive) asymptotic value of $G_{HF}^{PV}(k)$ (=0.111 for $k=1$ and 0.273 for $k=2.5$). Note that both $\mathrm{Re}G^1$ and $\mathrm{Re}G^{pr}$ tend to this asymptotic value and this guarantees that both local fields satisfy the third frequency moment sum rule to the same degree of accuracy. Regarding $\mathrm{Im}G^1$ and $\mathrm{Im}G^{pr}$, the noteworthy feature seems to be the large rise that occurs just before the cutoff at the upper characteristic frequency ω_s. The absence of a tail in $\mathrm{Im}G$ for large frequencies leads to the plasmon being undamped at long wavelengths in the present approximation. An important conclusion that can be drawn from these curves is that the local field varies quite appreciably with frequency: The real part varies by at least a factor of 2 over its range and also changes sign, while the imaginary part, although beginning from zero, attains values even greater than the real part. Therefore it seems quite unreasonable to approximate the entire dynamic local field by its static part, as done by Tripathy and Mandal[36,37] and by Toigo and Woodruff[12] in their calculations of various metallic properties.

In a recent paper Rao, Mandal, and Tripathy[39] have calculated numerically the local field $G^1(\vec{k},\omega)$ as a function of ω at $k=k_F$, and discussed the problem of its singularities. Their claim that there are no logarithmic singularities at ω_s is, in our view, incorrect for the reason that we have demonstrated unambiguously the existence of these singularities using analytical methods (in this respect we agree with the conclusions of Brosen *et al.*[33]). Also their plots of $G(\vec{k},\omega)$ vs ω are completely different from ours (Fig. 8, for $k=1$, solid line) even in the regions away from the singularities. Since our results conform to several independent internal checks, we feel that the numerical procedure used by these authors is seriously in error.

VII. DYNAMIC AND STATIC STRUCTURE FACTORS. PAIR CORRELATIONS

The differential inelastic scattering cross section for x rays and electrons is proportional to

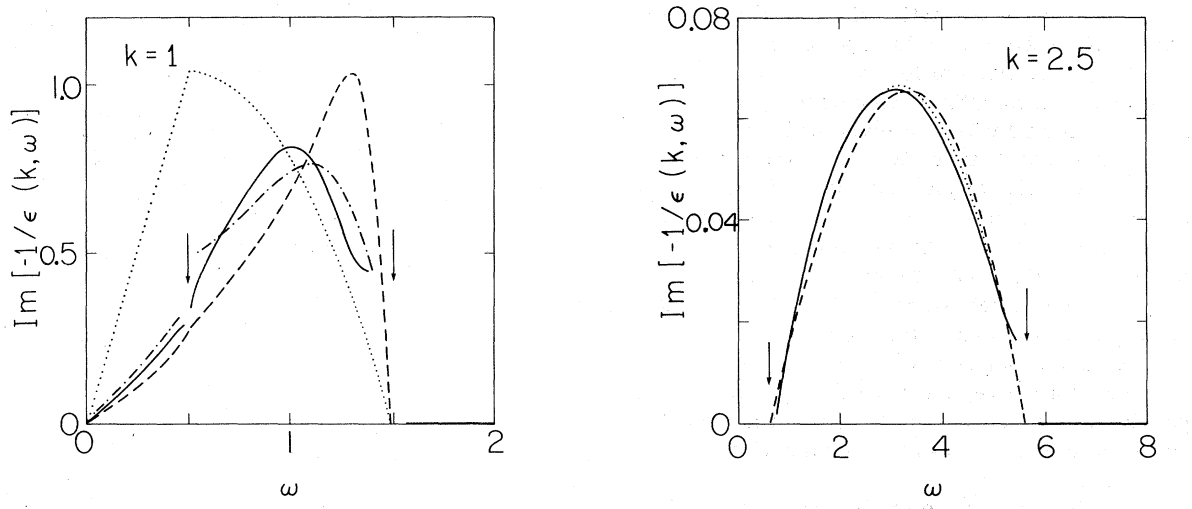

FIG. 9. Energy-loss function $\mathrm{Im}[-1/\epsilon(k,\omega)]$ [proportional to $S(k,\omega)$] at $r_s=2$; ——calculated in $G^{\mathrm{pr}}A$, - • - • - in G^1A, --- in RPA, • • • • for free-electron gas.

the dynamic structure factor

$$S(k,\omega)=-\frac{\hbar}{\pi n}\,\mathrm{Im}\,\chi(k,\omega)=\frac{3k^2}{4\alpha r_s}\,\mathrm{Im}\left(\frac{-1}{\epsilon(k,\omega)}\right), \quad (7.1)$$

where k is in units of k_F and S in $\hbar/2E_F$. The dielectric function (4.5) in terms of G is

$$\epsilon(k,\omega)=1+\frac{Q^0(k,\omega)}{1-G(k,\omega)Q^0(k,\omega)}. \quad (7.2)$$

In order to illustrate the effect of interaction in the first-order perturbation theory, we have plotted in Fig. 9 the function $\mathrm{Im}[-1/\epsilon(k,\omega)]$ in different approximations. There are two important points to note at $k=1$: (a) The shape of the dynamic structure factor in the perturbation theory $G^{\mathrm{pr}}A$ is more symmetrical than that in the RPA and (b) the peak position in the former is shifted to much lower energy than the latter. This behavior is in accord with the observation of Batson *et al.* for Al, Fig. 10. Of course, the first-order theory is unable to produce the tail in the high-frequency region which is due to multipair production. One should also note that the difference between the results of the two approximations $G^{\mathrm{pr}}A$ and G^1A are significant here. The same function is plotted in Fig. 9 for $k=2.5$ also. As expected, for such large momentum transfer the effect of interaction is tiny.

In Fig. 11 we have plotted the peak positions of $S(k,\omega)$ for a wide range of momentum transfers for $r_s=2$ in various approximations. Because of their considerable interest, we shall discuss these curves in somewhat greater detail. A striking feature to note is that the RPA dispersion curve (for values of $k>k_c$) lies much above that given by $G^{\mathrm{pr}}A$, i.e., in this region of k values RPA is a

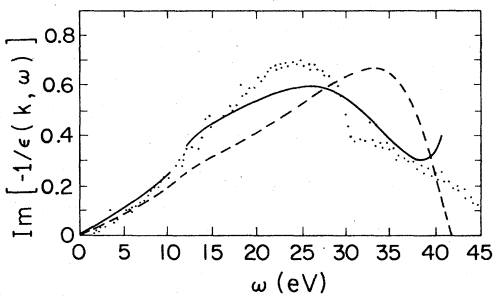

FIG. 10. Energy-loss function $\mathrm{Im}[-1/\epsilon(k,\omega)]$ for Al (at $r_s=2.07$), $k=2.0$ Å$^{-1}=1.14\,k_F$: ——calculated in $G^{\mathrm{pr}}A$, --- in RPA. Experimental points from Batson (Ref. 19).

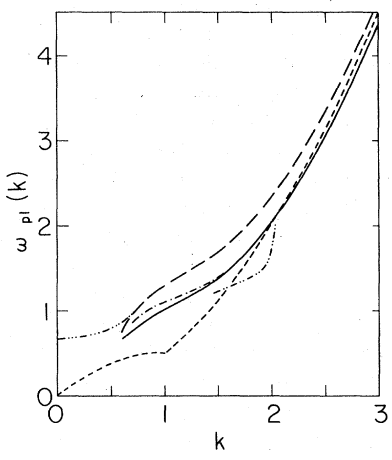

FIG. 11. Plasmon dispersion at $r_s=2$: – • • • – undamped plasmon (both in RPA and first-order theory); all other curves indicate peak position of $S(k,\omega)$. ——calculated in $G^{\mathrm{pr}}A$, - • - • - in G^1A, - • • - • • - with static part of G^1, ——— in RPA, --- for free-electron gas.

much poorer approximation than the first-order perturbation theory. In the region around $k=1$, the alternative first-order theory G^1A differs appreciably from $G^{pr}A$ (curve corresponding to G^1A agrees well with that given by Devreese *et al.*[40]). In order to investigate how important is the ω dependence of the first-order terms, we performed calculations using the static value of G^1 and obtained the dash-double-dot curve. This curve is identical with the one obtained by Tripathy *et al.*,[41] from which we conclude that these authors used the static value of their G, although this severe restriction is not mentioned in their paper.

In the small-k region ($k \leq 0.5$), the plasmon dispersion curve in $G^{pr}A$ and G^1A is practically the same as in RPA. This is in accord with experiment (see Sec. III).

The region around the critical wave vector k_c deserves special consideration. The plasmon frequency $\omega_{pl}(k)$ in $G^{pr}A$ is higher by 1.4% for $k=0.6$ and 3.1% for $k=0.7$ (3.5% in G^1A) than in RPA. Both the plasmon and the particle-hole continuum contribute to the total intensity; at small k it is predominantly the former, and closer to q_c it is the latter. For example at $k=0.5$, plasmon accounts for 85% of the total intensity (RPA value is 92%), while at $k=0.7$ the corresponding contribution is 42% (in RPA 53%). The intensity of the RPA plasmon drops to zero as k approaches k_c because of the logarithmic behavior of $\partial Q^0/\partial\omega$. Although we are unable to determine here the plasmon frequency in $G^{pr}A$ because it lies around ω_s (the singular region), we do find, however, that the intensity corresponding to it goes rapidly to zero. For $k \geq 1$ we find no "two-peak" structure[23] in our $S(k,\omega)$.

Higher-order terms, not included in the present theory, give rise to a finite width of the plasmon, which is obviously much less than the width of the particle-hole continuum. For a high-resolution (both in k and ω) experiment, in the range $0.5 < k < 0.7$, it should be possible to observe two separate peaks: one very narrow and the other quite broad, whose relative intensities change from being predominantly plasmon to predominantly particle-hole continuum. Actual experimental points of Batson *et al.*[19] in Al lie in between the two peaks as can be seen in Fig. 12.

The purpose of the above detailed discussion of the behavior of the plasmon and the particle-hole continuum contributions in the region below and close to q_c has been, in particular, to clarify confusing considerations made by Tripathy *et al.*[41] on this subject.

Because of the closeness of the theoretical dispersion curve with experiment, we are inclined to believe that the first-order perturbation theory

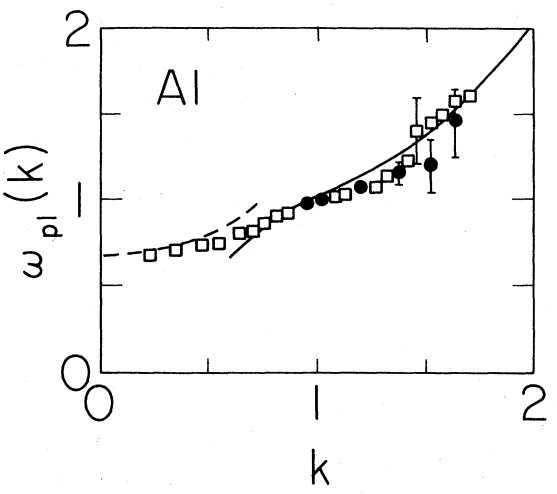

FIG. 12. Plasmon dispersion for Al (at $r_s=2$): --- undamped plasmon, —peak position of $S(k,\omega)$ calculated in $G^{pr}A$. Experimental points from Batson (Ref. 19).

is quite satisfactory and the role of the higher-order terms even at $r_s=2$ is not very significant. Nonetheless, the contribution of the first-order theory is very marked compared to that of the RPA.

In the region $0.7 < k < 1.3$, where $G^{pr}A$ and G^1A differ slightly from each other, experiment is in favor of the former (cf. Figs. 12 and 11).

The static structure factor $S(k)$ is given by

$$S(k)=\int_0^\infty d\omega\, S(k,\omega)=\frac{3k^2}{4\alpha r_s}\int_0^\infty d\omega\,\mathrm{Im}\left(\frac{-1}{\epsilon(k,\omega)}\right). \tag{7.3}$$

[In all the approximations considered here, the integration range in (7.3) may be limited from above by $\omega_s=k+k^2/2$, but at $k<k_c$ plasmon contribution must then be added separately.] Singularities in Q^1 at ω_s lead to integrable singularities in $S(k,\omega)$, therefore there was no need to exclude from integration the regions surrounding them, although they are difficult to handle in numerical work. The accuracy of numerical integration in (7.3) may be estimated by checking the fulfillment of the f-sum rule[3] [combine (3.14) and (7.1)]:

$$1=\frac{3}{2\alpha r_s}\int_0^\infty d\omega\,\omega\,\mathrm{Im}\left(\frac{-1}{\epsilon(k,\omega)}\right). \tag{7.4}$$

Both integrands in (7.3) and (7.4) are very similar and cause the same difficulties mentioned above.

In Fig. 13 we have plotted the calculated $S(k)$ in various approximations. The RPA result, although exact in the small-k region[3] where it has the form

$$S(k)=\frac{1}{2\omega_p(r_s)}k^2+O(k^4), \tag{7.5}$$

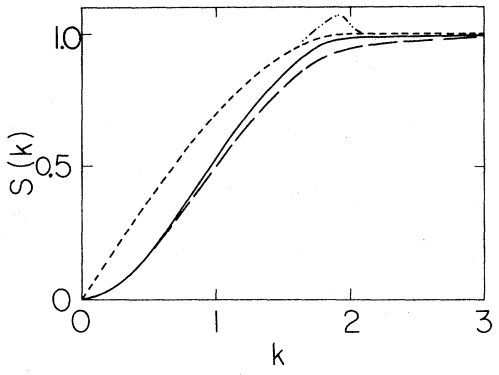

FIG. 13. Static structure factor $S(k)$ at $r_s=2$. ——calculated in $G^{pr}A$, – – – in RPA, – – – for free-electron gas $[S_{HF}(k)]$, – · · – · · – with static part of G^1.

differs considerably from that of $G^{pr}A$ (full line) in the region at larger k. For large k, the structure factor has the following expansion[42]:

$$S(k)=1+\frac{C}{k^4}+O\left(\frac{1}{k^6}\right). \tag{7.6}$$

From Eqs. (7.6), (7.3), and (7.2) it follows that

$$C=\lim_{k\to\infty}k^4\left[\frac{3k^2}{4\alpha r_s}\times\int_0^\infty d\omega\,\mathrm{Im}\left(\frac{Q^0(k,\omega)}{1+[1-G(k,\omega)]Q^0(k,\omega)}\right)-1\right]. \tag{7.7}$$

Expanding the denominator and noting that the leading term is canceled exactly with -1, one obtains

$$C=\lim_{k\to\infty}\frac{3k^6}{4\alpha r_s}\int_0^\infty d\omega\,\mathrm{Im}[-(1-G)(Q^0)^2+(1-G)^2(Q^0)^3-\cdots]. \tag{7.8}$$

On examining the k dependence, it can be shown that only the first term in square brackets in (7.8) contributes to C. In both $G^{pr}A$ and G^1A one gets the same value of C:

$$C=\frac{3}{4\alpha r_s}\left[-\lim_{k\to\infty}k^6\int_0^\infty d\omega\,\mathrm{Im}(Q^0)^2+\lim_{k\to\infty}k^6\int_0^\infty d\omega\,\mathrm{Im}(Q^1)\right]. \tag{7.9}$$

The above contributions can be easily calculated using integral representations of Q^1 (2.3), (2.4) and Q^0 (2.1), performing an integration over frequencies first and taking the large-k limit. The result is

$$C=\frac{8\alpha r_s}{3\pi}(-1+\tfrac{1}{2}), \tag{7.10}$$

which is in agreement with Brosens *et al.*[43] The first term in (7.10) corresponds to the first term in (7.9), and therefore gives the value of C in RPA, while the contribution from Q^1 diagrams reduces the RPA C by half. It is interesting that self-energy diagrams of Q^1 do not contribute to C (this is similar to the fact that self-energy diagrams do not contribute to the second-order correlation energy).

Once more we should emphasize the importance of the dynamical aspect of our calculations. If $S(k)$ is calculated with the static part of G^1 only (dash-double-dotted line in Fig. 13) a large peak appears at $k\approx 2$. This curve is the same as that obtained by Tripathy *et al.*,[37] showing that their calculations were restricted to the use of the static part of their G. This peak becomes more pronounced at higher r_s. Although we consider it unjustifiable to apply the first-order theory to higher r_s, we repeated the calculation of $S(k)$ at $r_s=6$ using both the static and dynamic G^1 for the sake of comparison with the result with static G^1 of Ref. 37. With static G^1 one obtains a peak in $S(k)$ as high as 1.3 at $k=1.95$, while dynamic G^1 gives a rather smooth curve with a maximum of 0.95 at $k=1.95$. We give these details in order to clearly demonstrate that all speculations of Tripathy *et al.*,[37] such as "incipient Bragg peak," connected with the above-mentioned peak, are spurious, and are based on an unjustified replacement of the dynamic $G^1(k,\omega)$ by its static value $G^1(k,0)$.

We shall now consider the pair correlation function $g(r)$ given by

$$g(r)=1+\frac{3}{8\pi}\int d^3k[S(k)-1]\exp(i\vec{k}\cdot\vec{r}), \tag{7.11}$$

where r is in units of $1/k_F$. Its value for $r=0$ is

$$g(0)=1+\tfrac{3}{2}\int dk\,k^2[S(k)-1]. \tag{7.12}$$

In Fig. 14 we show the r_s dependence of $g(0)$. One

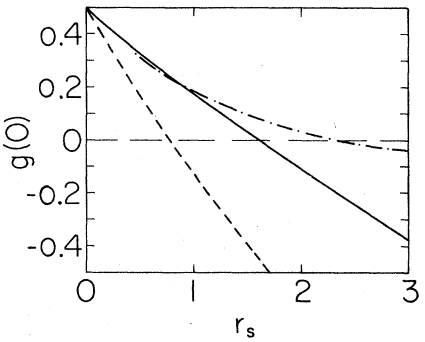

FIG. 14. Pair correlation function at zero distance: ——calculated in $G^{pr}A$, – – – in RPA, – · – · – in VS theory (Ref. 15).

notices a marked improvement in the value of $g(0)$ due to Q^1 contributions as compared with the RPA value. The initial part of the curve agrees well with the exact expansion formula (for $r_s \to 0$) given Kimball[44]:

$$g(0) = \tfrac{1}{2}\frac{\alpha}{5\pi}(\pi^2 + 6\ln 2 - 3)r_s - \left(\frac{3\alpha}{2\pi}\right)^2\left(3 - \frac{\pi^2}{4}\right)r_s^2 \ln r_s + O(r_s^2)\,. \tag{7.13}$$

For example, at $r_s = 0.5$ our $g(0)$ is only 4% higher than one calculated according to (7.12), and their difference diminishes to zero with decreasing r_s. The results of G^1A are very close to those of $G^{pr}A$, only slightly lower at larger r_s (e.g., $g(0) = -0.16$ at $r_s = 2$ in G^1A, compared to -0.10 in $G^{pr}A$).

It is interesting that the knowledge of large-k expansion for $S(k)$ [Eq. (7.6)] allows one to calculate from (7.11) the derivative of the pair correlation function, as was shown by Kimball[42]:

$$g'(0) = \left(\frac{\partial g(r)}{\partial r}\right)_{r=0} = \frac{3\pi}{8}\lim_{k\to\infty}\{k^4[I - S(k)]\} = -\frac{3\pi}{8}C\,. \tag{7.14}$$

This property, when combined with the following exact relation due to Kimball[42] (valid for particles interacting via Coulomb forces):

$$\frac{1}{\alpha r_s}g'(0) = g(0) \tag{7.15}$$

provides a new check of self-consistency for any approximate $S(k)$. The left-hand side of (7.15) may be calculated from (7.14), and the right-hand side from (7.12), and compared to see if they are equal. Using (7.10) and (7.14), in the $G^{pr}A$ (and G^1A as well) we obtain

$$\frac{1}{\alpha r_s}g'(0) = \frac{1}{2}, \tag{7.16}$$

which fulfills the identity (7.15) in the $r_s \to 0$ limit only. Such approximate fulfillment of the Kimball relation is in accord with the approximate character of the first-order theory. In view of the above considerations we do not agree with the claim of Brosens *et al.*[43] that the Kimball relation is exactly satisfied by their theory (G^1A in our notation). In making their claim they used the relation

$$g(0) = 1 - \tfrac{3}{2}\lim_{k\to\infty} G(k,0)\,, \tag{7.17}$$

which was derived by Niklasson for an exact theory, but it may be satisfied only approximately in G^1A and $G^{pr}A$. Indeed, from high-k expansion $Q^1(k,0) \sim 1/k^4$, with coefficients determined by Geldart and Taylor,[14] one immediately obtains

$$\lim_{k\to\infty} G^{pr}(k,0) = \lim_{k\to\infty} G^1(k,0) = \tfrac{1}{3}\,, \tag{7.18}$$

which gives for the right-hand side of (7.17) the value $\frac{1}{2}$, while the left-hand side is r_s dependent and is equal to $\frac{1}{2}$ only in the limit $r_s \to 0$. Although both Kimball's and Niklasson's relations are satisfied only approximately, it so happens that the left-hand side of (7.15) is equal to the right-hand side of (7.17), which constitutes the actual interpretation of the statement of Brosens *et al.*[43]

According to definition (7.11), $g(r)$ may in principle be calculated for any argument r. Since we are able to calculate $S(k)$ only at a limited number of points k and with finite accuracy, we need some interpolating and smoothing procedure applied to $S(k)$ before the numerical integration can be accomplished. Details are given in Appendix C. Results of the integration are shown in Fig. 15. The $G^{pr}A$ results are given as a dash-dotted line for $r_s = 1$ and a dashed line for $r_s = 2$. For comparison the RPA results for $r_s = 1$ are shown as a dotted line. It is interesting that, except for $g_{HF}(r)$, pair correlation function behaves almost linearly, with the initial slope given by (7.14), over a wide range of r values (up to ≈ 1.5), then bends slightly to approach $g_{HF}(r)$. For $r > 4$, $g(r)$ is practically equal to 1, although when magnified, Friedel oscillations can be seen (see insert Fig. 15).

In the paper of Mandal *et al.*[36] $g(r)$ and related quantities are calculated in the approximation equivalent to G^1A, but restricted to using the static values of G^1. As we mentioned earlier in connection with $S(k)$, this restriction severely distorts

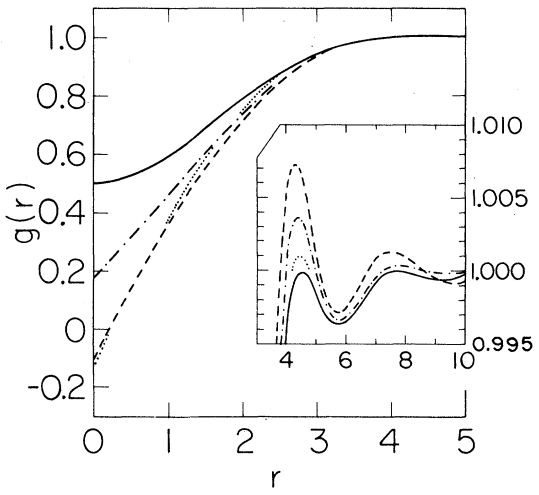

FIG. 15. Pair correlation function vs distance r (in k_F^{-1}): —— for free-electron gas (g_{HF}), - · - · - calculated in $G^{pr}A$ at $r_s = 1$, · · · · in RPA at $r_s = 1$, - - - in $G^{pr}A$ at $r_s = 2$.

the results of the calculations. Large oscillations in $g(r)$ calculated in Ref. 36 are again due to the use of a static G^1 (e.g., at $r_s=3$ they observe a maximum equal to 1.03, while using dynamic G^1 we obtain 1.008 only). For higher values of r_s the value of the maximum in $g(r)$ becomes quite large.[36] This is again due to the use of the first-order perturbation theory in a region of densities where it is not valid and due to the use of a static G^1. We therefore believe that the conclusions and remaining results of Mandal *et al.*[36] are invalid.

VIII. CONCLUSION

Our extensive investigation of the first-order perturbation theory demonstrates that it is a significant improvement over the RPA for a wide variety of calculated properties. We have also seen that it is very important to keep the ω dependence of the local field factor $G(k,\omega)$.

Although the perturbation theory is strictly valid in the small r_s region, our calculations nevertheless show that even for r_s as large as 2 the results agree fairly well with experiment. This indicates that the first-order perturbation theory has a wider range of validity then one might have supposed.

The first-order theory is unable to give either the damping of the plasmon or the high-frequency tail of the dynamical structure factor. Both these effects are the result of multiparticle excitations, a topic which will be dealt with in a subsequent paper.

ACKNOWLEDGMENTS

This work was supported in part under National Science Foundation-Materials Research Laboratories program through the Material Research Center of Northwestern University (Grant No. DMR 76-80847) and in part by the National Science Foundation Grant No. DMR 77-09937.

APPENDIX A: EVALUATION OF $\mathrm{Im}F^{\mathrm{SE}}$

We wish to evaluate the imaginary part of the function

$$F^{\mathrm{SE}}(\vec{k},\omega)=-\tfrac{1}{2}\int d^3p\int d^3p'\frac{1}{(\vec{p}'-\vec{p})^2}\frac{(n^0_{\vec{p}}-n^0_{\vec{p}+\vec{k}})(n^0_{\vec{p}'}-n^0_{\vec{p}'+\vec{k}})}{(\omega+i\eta+\omega_{\vec{p}}-\omega_{\vec{p}+\vec{k}})^2}, \tag{A1}$$

where

$$\omega_{\vec{q}}=\tfrac{1}{2}\vec{q}^2, n^0_{\vec{q}}=\theta(1-\vec{q}^2).$$

Expressing the squared denominator as a derivative (i.e., using the identity $1/(\omega+x)^2=-(\partial/\partial\omega)[1/(\omega+x)]$) and applying the Dirac identity we have

$$\mathrm{Im}F^{\mathrm{SE}}(\vec{k},\omega)=-\frac{\pi}{2}\frac{\partial}{\partial\omega}\int d^3p\int d^3p'\frac{1}{(\vec{p}-\vec{p}')^2}(n^0_{\vec{p}}-n^0_{\vec{p}+\vec{k}})(n^0_{\vec{p}'}-n^0_{\vec{p}'+\vec{k}})\,\delta(\omega+\omega_{\vec{p}}-\omega_{\vec{p}+\vec{k}}). \tag{A2}$$

Introduce the function

$$f(q)=\int d^3p\frac{n^0_{\vec{p}}}{(\vec{p}-\vec{q})^2}, \tag{A3}$$

which depends only on the magnitude of $\vec{q}$. This function is easliy calculated to be

$$f(q)=4\pi f_L(q)=4\pi\left(\tfrac{1}{2}+\frac{1-q^2}{4q}\ln\left|\frac{1+q}{1-q}\right|\right). \tag{A4}$$

Equation (A2) can now be written as

$$\mathrm{Im}F^{\mathrm{SE}}=\mathrm{Im}(F^{\mathrm{SE}}_1+F^{\mathrm{SE}}_2+F^{\mathrm{SE}}_3+F^{\mathrm{SE}}_4),$$

where

$$\begin{aligned}\mathrm{Im}F^{\mathrm{SE}}_{1,2}(\vec{k},\omega)&=-\frac{\pi}{2}\frac{\partial}{\partial\omega}\int d^3p\,n^0_{\vec{p}}f(p)\,\delta(\omega\pm\omega_{\vec{p}}\mp\omega_{\vec{p}+\vec{k}})\\ \mathrm{Im}F^{\mathrm{SE}}_{3,4}(\vec{k},\omega)&=\frac{\pi}{2}\frac{\partial}{\partial\omega}\int d^3p\,n^0_{\vec{p}}f(|\vec{p}+\vec{k}|)\,\delta(\omega\pm\omega_{\vec{p}}\mp\omega_{\vec{p}+\vec{k}}).\end{aligned} \tag{A5}$$

It is easily seen that

$$\mathrm{Im}F^{\mathrm{SE}}_{2,4}(\vec{k},\omega)=-\mathrm{Im}F^{\mathrm{SE}}_{1,3}(\vec{k},-\omega). \tag{A6}$$

Thus

$$\mathrm{Im}F^{\mathrm{SE}}(\vec{k},\omega)=\mathrm{Im}[F_1^{\mathrm{SE}}(\vec{k},\omega)-F_1^{\mathrm{SE}}(\vec{k},-\omega)+F_3^{\mathrm{SE}}(\vec{k},\omega)-F_3^{\mathrm{SE}}(\vec{k},-\omega)]\,, \tag{A7}$$

and we need calculate only $\mathrm{Im}F_1^{\mathrm{SE}}$ and $\mathrm{Im}F_3^{\mathrm{SE}}$. These functions can be evaluated quite straightforwardly by adopting the usual spherical polar coordinate system. We find that

$$\mathrm{Im}F_1^{\mathrm{SE}}(k,\omega)=\frac{4\pi^3}{k^2}\nu_+\theta(1-\nu_+^2)f_L(\nu_+)\,, \tag{A8}$$

$$\mathrm{Im}F_3^{\mathrm{SE}}(\vec{k},\omega)=\frac{4\pi^3}{k^2}\theta(1-\nu_+^2)[\nu_-f_L(\nu_-)+kf_L(1+2\omega)^{1/2}]\,, \tag{A9}$$

with

$$\nu_\pm=\pm\frac{\omega}{k}-\frac{k}{2}\,. \tag{A10}$$

On using (A8) and (A9) in (A7) we get

$$\mathrm{Im}F^{\mathrm{SE}}(\vec{k},\omega)=\frac{4\pi^3}{k^2}\theta(1-\nu_+^2)[\nu_+f_L(\nu_+)+\nu_-f_L(\nu_-)+kf_L(1+2\omega)^{1/2}]-\frac{4\pi^3}{k^2}\theta(1-\nu_-^2)[\nu_+f_L(\nu_+)+\nu_-f_L(\nu_-)+kf_L(1-2\omega)^{1/2}]\,. \tag{A11}$$

If we define

$$\Phi^{\mathrm{SE}}(\nu,k)=\nu f_L(\nu)-(k+\nu)f_L(k+\nu)+kf_L(k^2+2k\nu+1)^{1/2}$$

and remember that $\nu_+=-(\nu_-+k)$, we see immediately that (A11) goes over into the expression (2.13) given in the text.

APPENDIX B: EVALUATION OF $\mathrm{Im}F^{\mathrm{SE}}$

The first-order exchange diagram leads to the integral

$$F^{\mathrm{Ex}}(\vec{k},\omega)=\tfrac{1}{2}\int\frac{d^3p\,d^3p'}{(\vec{p}-\vec{p}')^2}\frac{(n^0_{\vec{p}}-n^0_{\vec{p}+\vec{k}})(n^0_{\vec{p}'}-n^0_{\vec{p}'+\vec{k}})}{(\omega+i\eta+\omega_{\vec{p}}-\omega_{\vec{p}+\vec{k}})(\omega+i\eta+\omega_{\vec{p}'}-\omega_{\vec{p}'+\vec{k}})}\,. \tag{B1}$$

The imaginary part of this expression is

$$\mathrm{Im}F^{\mathrm{Ex}}(\vec{k},\omega)=\tfrac{1}{2}\int\frac{d^3p\,d^3p'}{(\vec{p}-\vec{p}')^2}(n^0_{\vec{p}}-n^0_{\vec{p}+\vec{k}})(n^0_{\vec{p}'}-n^0_{\vec{p}'+\vec{k}})$$
$$\times\left[-\pi\delta(\omega+\omega_{\vec{p}}-\omega_{\vec{p}+\vec{k}})P\frac{1}{\omega+\omega_{\vec{p}'}-\omega_{\vec{p}'+\vec{k}}}-P\frac{1}{\omega+\omega_{\vec{p}}-\omega_{\vec{p}+\vec{k}}}\pi\delta(\omega+\omega_{\vec{p}'}-\omega_{\vec{p}'+\vec{k}})\right]. \tag{B2}$$

By interchanging the dummy variables $\vec{p}$ and $\vec{p}'$ in the second term one sees that it is identical to the first so that

$$\mathrm{Im}F^{\mathrm{Ex}}(\vec{k},\omega)=-\pi\int\frac{d^3p\,d^3p'}{(\vec{p}-\vec{p}')^2}(n^0_{\vec{p}}-n^0_{\vec{p}+\vec{k}})(n^0_{\vec{p}'}-n^0_{\vec{p}'+\vec{k}})\delta(\omega+\omega_{\vec{p}}-\omega_{\vec{p}+\vec{k}})P\frac{1}{\omega+\omega_{\vec{p}'}-\omega_{\vec{p}'+\vec{k}}}\,. \tag{B3}$$

Define the functions

$$\mathrm{Im}F_1^{\mathrm{Ex}}(\vec{k},\omega)=-\pi\int d^3p\,n^0_{\vec{p}}\delta(\omega+\omega_{\vec{p}}-\omega_{\vec{p}+\vec{k}})\int\frac{d^3p'}{(\vec{p}-\vec{p}')^2}n^0_{\vec{p}'}P\frac{1}{\omega+\omega_{\vec{p}'}-\omega_{\vec{p}'+\vec{k}}}$$
$$\mathrm{Im}F_2^{\mathrm{Ex}}(\vec{k},\omega)=\pi\int d^3p\,n^0_{\vec{p}}\delta(\omega+\omega_{\vec{p}}-\omega_{\vec{p}+\vec{k}})\int\frac{d^3p'}{(\vec{p}'+\vec{k}+\vec{p})^2}n^0_{\vec{p}'}P\frac{1}{\omega+\omega_{\vec{p}'+\vec{k}}-\omega_{\vec{p}'}}\,. \tag{B4}$$

In terms of them (B3) can be written compactly as

$$\mathrm{Im}F^{\mathrm{Ex}}(\vec{k},\omega)=\mathrm{Im}[F_1^{\mathrm{Ex}}(\vec{k},\omega)-F_1^{\mathrm{Ex}}(\vec{k},-\omega)+F_2^{\mathrm{Ex}}(\vec{k},\omega)-F_2^{\mathrm{Ex}}(\vec{k},-\omega)]\,. \tag{B5}$$

In both $\mathrm{Im}F_1^{\mathrm{Ex}}$ and $\mathrm{Im}F_2^{\mathrm{Ex}}$ the integral over $\vec{p}'$ has the general form

$$\Phi_1(a,\vec{k}_1,\vec{k}_2)=\int d^3p\,\frac{n^0_{\vec{p}}}{(\vec{p}-\vec{k}_1)^2}P\frac{1}{a-\vec{k}_2\cdot\vec{p}}\,. \tag{B6}$$

We can regard this integral as the real part of

the complex function

$$\Phi(a,\vec{k}_1,\vec{k}_2)=\int d^3p\,\frac{n^0_{\vec{p}}}{(\vec{p}-\vec{k}_1)^2}\,\frac{1}{(a+i\eta-\vec{k}_2\cdot\vec{p})}\,, \tag{B7}$$

$$\eta=0^+,$$

$$\Phi_1(a,\vec{k}_1,\vec{k}_2)=\mathrm{Re}\Phi(a,\vec{k}_1,\vec{k}_2)\,. \tag{B8}$$

As usual, we will first calculate $\mathrm{Im}\Phi$ and then obtain $\mathrm{Re}\Phi$ through Hilbert transformation. It is evident that Φ depends only on the lengths of the vectors $\vec{k}_1$ and $\vec{k}_2$ and the angle between them. The dependence on $\vec{k}_2$ may be further simplified:

$$\Phi(a,\vec{k}_1,\vec{k}_2)=\frac{\pi}{k_2}\,\tilde{\Phi}\left(\frac{a}{k_2},\frac{\vec{k}_1\cdot\vec{k}_2}{k_2},k_1^2\right),$$

where

$$\tilde{\Phi}\left(\xi,\frac{\vec{k}_1\cdot\vec{k}_2}{k_2},k_1^2\right)=\frac{1}{\pi}\int\frac{d^3p}{(\vec{p}-\vec{k}_1)^2}n^0_{\vec{p}}\,\frac{1}{(\xi+i\eta-\vec{k}_2\cdot\vec{p}/k_2)}\,. \tag{B9}$$

Introduce a coordinate system with the z axis along $\vec{k}_2$ and x axis in the plane $(\vec{k}_1,\vec{k}_2)$. If $c_1=\vec{k}_1\cdot\vec{k}_2/k_1k_2$ and $s_1=(1-c_1^2)^{1/2}$ then

$$\vec{k}_2=k_2(0,0,1),\quad \vec{k}_1=k_1(s_1,0,c_1),$$
$$\vec{p}=p((1-t^2)^{1/2}\cos\varphi,\,(1-t^2)^{1/2}\sin\varphi,t)\,. \tag{B10}$$

$t=\cos\theta$ and φ specify the polar coordinates of $\vec{p}$ with respect to the chosen set of axes. Equation (B9) now becomes

$$\tilde{\Phi}\left(\xi,\frac{\vec{k}_1\cdot\vec{k}_2}{k_2},k_1^2\right)=\frac{1}{\pi}\int_0^1 dp\,p^2\int_{-1}^1\frac{dt}{\xi+i\eta-pt}\mathrm{P}\int_0^{2\pi}\frac{d\varphi}{p^2+k_1^2-2k_1pc_1t-2k_1ps_1(1-t^2)^{1/2}\cos\varphi}\,. \tag{B11}$$

The principal value has been introduced in order to handle properly the singular but integrable Coulomb potential. Now use the formula

$$\mathrm{P}\int_0^{2\pi}\frac{d\varphi}{\alpha-\beta\cos(\varphi)}=\frac{2\pi\,\mathrm{sgn}(\alpha)\theta(\alpha^2-\beta^2)}{(\alpha^2-\beta^2)^{1/2}} \tag{B12}$$

to evaluate the φ integral in (B11), where, in our case, $\alpha=p^2+k_1^2-2pk_1c_1t$, $\beta=2pk_1s_1(1-t^2)^{1/2}$. From the inequality $(\vec{p}-\vec{k}_1)^2\geq 0$, which in terms of above variables is $\alpha-\beta\cos(\varphi)\geq 0$, it follows that $\alpha\geq|\beta|\geq 0$. Therefore the θ and sgn functions are always unity in this case. If we set $W=\alpha^2-\beta^2$ then (B11) becomes

$$\tilde{\Phi}=\int_0^1 2p^2dp\int_{-1}^{+1}\frac{dt}{\sqrt{W}(\xi+i\eta-pt)} \tag{B13}$$

and

$$\mathrm{Im}\tilde{\Phi}=-\pi\int_0^1 2p^2dp\int_{-1}^{+1}\frac{dt}{\sqrt{W}}\delta(\xi-pt)\,. \tag{B14}$$

The t integral is easily evaluated. In the p integral we switch variables to $x=p^2$ and obtain

$$\mathrm{Im}\tilde{\Phi}=-\pi\theta(1-\xi^2)\int_{\xi^2}^1\frac{dx}{\sqrt{W}}\,. \tag{B15}$$

In the above integral we have to evaluate W with $p^2=x$ and $pt=\xi$. Using the notation $\mu=\vec{k}_1\cdot\vec{k}_2/k_2$ and $\gamma=k_1^2$ and evaluating W we obtain

$$W(\xi,\mu,\gamma,x)=(x-x_0)^2+B^2\,, \tag{B16}$$

where

$$x_0(\xi,\mu,\gamma)=\gamma+2\mu(\xi-\mu) \tag{B17}$$

and

$$B^2(\xi,\mu,\gamma)=4(\gamma-\mu^2)(\xi-\mu)^2\,. \tag{B18}$$

The integral in (B15) can now be evaluated to yield

$$\mathrm{Im}\tilde{\Phi}=-\pi\theta(1-\xi^2)\ln\left(\frac{N(\xi,\mu,\gamma)}{A_1(\xi,\mu)}\right), \tag{B19}$$

where

$$N(\xi,\mu,\gamma)=1-x_0+[(1-x_0)^2+B^2]^{1/2}$$
$$=1-\gamma-2\mu(\xi-\mu)+(W(\xi,\mu,\gamma,1))^{1/2} \tag{B20}$$

and

$$A_1(\xi,\mu)=\xi^2-x_0+[(\xi^2-x_0)^2+B^2]^{1/2}$$
$$=2(\xi-\mu)^2\,. \tag{B21}$$

It is evident that $N\geq 0$ and $A_1\geq 0$ in general.

$\mathrm{Re}\tilde{\Phi}$ is given by the Hilbert transform

$$\mathrm{Re}\tilde{\Phi}(\xi,\mu,\gamma)=-\frac{1}{\pi}\mathrm{P}\int_{-\infty}^{\infty}\frac{\mathrm{Im}\tilde{\Phi}(\xi',\mu,\gamma)}{\xi-\xi'}d\xi'\,. \tag{B22}$$

On using (B19), (B22), (B8), and (B9) we obtain

$$\Phi_1(a,\vec{k}_1,\vec{k}_2)=\frac{\pi}{k_2}\mathrm{P}\int_{-1}^{+1}\frac{d\xi'}{(a/k_2-\xi')}\ln\left(\frac{N(\xi',\vec{k}_1\cdot\vec{k}_2/k_2,k_1^2)}{A_1(\xi',\vec{k}_1\cdot\vec{k}_2/k_2)}\right). \tag{B23}$$

Equation (B4) can be expressed in terms of (B23) to give

$$\mathrm{Im}(F_1^{\mathrm{Ex}}+F_2^{\mathrm{Ex}})=-\pi\int d^3p\,n^0_{\vec{p}}\,\delta(\omega-\tfrac{1}{2}k^2-\vec{p}\cdot\vec{k})E(\omega,k^2,p^2,\vec{p}\cdot\vec{k})\,, \tag{B24}$$

where

$$E(\omega,k^2,p^2,\vec{p}\cdot\vec{k})=\Phi_1(\omega-\tfrac{1}{2}k^2,\vec{p},\vec{k})-\Phi_1(\omega+\tfrac{1}{2}k^2,\vec{p}+\vec{k},\vec{k})\,. \tag{B25}$$

To evaluate (B24) we use polar coordinates with the axis along $\vec{k}$. Switching variables from p to $\gamma=p^2$ and recalling that $\nu_+=\omega/k-\frac{1}{2}k$ the integral becomes

$$\begin{aligned}\mathrm{Im}(F_1^{Ex}+F_2^{Ex})&=-\frac{\pi^2}{k}\theta(1-\nu_+^2)\int_{\nu_+^2}^{1}d\gamma\,E(\omega,k^2,\gamma,k\nu_+)\\&=-\frac{\pi^3}{k^2}\theta(1-\nu_+^2)\int_{\nu_+^2}^{1}d\gamma\left[\mathrm{P}\int_{-1}^{+1}\frac{d\xi}{\nu_+-\xi}\ln\left(\frac{N(\xi,\nu_+,\gamma)}{A_1(\xi,\nu_+)}\right)\right.\\&\qquad\left.-\mathrm{P}\int_{-1}^{+1}\frac{d\xi}{\nu_++k-\xi}\ln\left(\frac{N(\xi,\nu_++k,\gamma+k^2+2k\nu_+)}{A_1(\xi,\nu_++k)}\right)\right].\end{aligned}$$

On changing the order of integration we get

$$\mathrm{Im}(F_1^{Ex}+F_2^{Ex})=-\frac{\pi^3}{k^2}\theta(1-\nu_+^2)\,\mathrm{P}\int_{-1}^{+1}d\xi\left(\frac{T_1(\xi,\nu_+)}{\nu_+-\xi}-\frac{T_3(\xi,\nu_+,k)}{\nu_++k-\xi}\right), \tag{B26}$$

where

$$T_1(\xi,\nu_+)=\int_{\nu_+^2}^{\nu_+^2+(1-\nu_+^2)}d\gamma\ln\left(\frac{N(\xi,\nu_+,\gamma)}{A_1(\xi,\nu_+)}\right), \tag{B27}$$

and

$$T_3(\xi,\nu_+,k)=\int_{(\nu_++k)^2}^{(\nu_++k)^2+(1-\nu_+^2)}d\gamma\ln\left(\frac{N(\xi,\nu_++k,\gamma)}{A_1(\xi,\nu_++k)}\right). \tag{B28}$$

Introduce

$$L(\gamma_0,\xi,\mu)=\int^{\gamma_0}d\gamma\ln[N(\xi,\mu,\gamma)] \tag{B29}$$

and

$$\begin{aligned}T(\xi,\mu,1-\nu_+^2)&=L(\mu^2+(1-\nu_+^2),\xi,\mu)\\&\quad-L(\mu^2,\xi,\mu)-(1-\nu_+^2)\ln[A_1(\xi,\mu)]\,.\end{aligned} \tag{B30}$$

Then

$$\begin{aligned}T_1(\xi,\nu_+)&=T(\xi,\nu_+,1-\nu_+^2),\\T_3(\xi,\nu_+,k)&=T(\xi,\nu_++k,1-\nu_+^2)\,.\end{aligned} \tag{B31}$$

Further let

$$G_1(\nu)=\tfrac{1}{4}\mathrm{P}\int_{-1}^{+1}d\xi\frac{T(\xi,\nu,1-\nu^2)}{\nu-\xi} \tag{B32}$$

and

$$G_2(x_1,x_2)=\tfrac{1}{4}\mathrm{P}\int_{-1}^{+1}d\xi\frac{T(\xi,x_1,x_2)}{\xi-x_1}\,. \tag{B33}$$

With these definitions (B5) can finally be written as

$$\begin{aligned}\mathrm{Im}F^{Ex}(\vec{k},\omega)&=\frac{4\pi^3}{k^2}\theta(1-\nu_+^2)[-G_1(\nu_+)+G_2(\nu_++k,1-\nu_+^2)]\\&\quad-\frac{4\pi^3}{k^2}\theta(1-\nu_-^2)[-G_1(\nu_-)\\&\qquad+G_2(\nu_-+k,1-\nu_-^2)]\,.\end{aligned} \tag{B34}$$

The remaining task is the evaluation of the functions $G_1(\nu)$ and $G_2(x_1,x_2)$.

Evaluation of $G_1(\nu)$. We will first obtain an explicit expression for the function $L(\gamma_0,\xi,\mu)$ defined in (B29). Since the algebra is fairly straightforward we only show a few steps along the way before giving the final result.

Rewrite N (B20) as

$$\begin{aligned}N(\xi,\mu,\gamma)&=A_1(\xi,\mu)-[\gamma+A_3(\xi,\mu)]\\&\quad+\{[\gamma+A_3(\xi,\mu)]^2+A_2(\xi,\mu)\}^{1/2},\end{aligned} \tag{B35}$$

where

$$A_2(\xi,\mu)=4(\xi-\mu)^2(1-\xi^2)\,, \tag{B36}$$

and

$$A_3(\xi,\mu)=2\xi(\xi-\mu)-1; \tag{B37}$$

$$\begin{aligned}L(\gamma_0,\xi,\mu)&\equiv H(A_1,A_2,A_3,\gamma_0)\\&=\int^{\gamma_0}d\gamma\ln\{A_1-(\gamma+A_3)\\&\qquad+[(\gamma+A_3)^2+A_2]^{1/2}\}\,.\end{aligned}$$

Change the variable to $y(\gamma)=A_1-(\gamma+A_3)+[(\gamma+A_3)^2+A_2]^{1/2}$,

$$\begin{aligned}H(A_1,A_2,A_3,\gamma_0)&=\int^{y(\gamma_0)}d\gamma\left(-\tfrac{1}{2}-\frac{A_2}{2(y-A_1)^2}\right)\ln y\\&=\left(-\tfrac{1}{2}+\frac{A_2}{2A_1}\frac{1}{(y_0-A_1)}\right)y_0\ln y_0\\&\quad+\tfrac{1}{2}y_0-\frac{A_2}{2A_1}\ln(y_0-A_1)\,,\end{aligned} \tag{B38}$$

where

$$y_0=A_1-(\gamma_0+A_3)+[(\gamma_0+A_3)^2+A_2]^{1/2}\,. \tag{B39}$$

Using (B38) we find that

$$\begin{aligned}L(\nu_+^2,\xi,\nu_+)&=1-2\nu_+\xi+\nu_+^2\\&\quad-(1-\xi^2)\ln[2(1-\xi^2)]\,,\end{aligned} \tag{B40}$$

$$L(1,\xi,\nu_+)=(1-\nu_+^2)\ln|2(\xi-\nu_+)(s-\nu_+)|+(\xi-\nu_+)(s-\nu_+)-(1-\xi^2)\ln|2(\xi-\nu_+)(s-\xi)|, \tag{B41}$$

$$\begin{aligned}T_1&=T(\xi,\nu_+,1-\nu_+^2)=L(1,\ \xi,\ \nu_+)-L(\nu_+^2,\xi,\nu_+)-(1-\nu_+^2)\ln[2(\xi-\nu_+)^2]\\&=(\xi-\nu_+)s-1+\nu_+\xi+(-2+\nu_+^2+\xi^2)\ln|\xi-\nu_+|+(1-\nu_+^2)\ln|s-\nu_+|\\&\quad-(1-\xi^2)\ln|s-\xi|+(1-\xi^2)\ln(1-\xi^2).\end{aligned} \tag{B42}$$

The notation $s=\mathrm{sgn}(\xi-\nu_+)$ has been used above.

Now we calculate $G_1(\nu)$ from (B32):

$$G_1(\nu)=-\tfrac{1}{4}\mathrm{P}\int_{-1}^{+1}d\xi\frac{T_A+T_B+T_C+T_D+T_E}{\xi-\nu}, \tag{B43}$$

where

$$\begin{aligned}&T_A(\xi,\nu)=(\xi-\nu)s-1+\nu\xi,\quad T_B(\xi,\nu)=(-2+\nu^2+\xi^2)\ln|\xi-\nu|,\\&T_C(\xi,\nu)=(1-\nu^2)(\ln|s-\nu|-\ln|s-\xi|),\quad T_D(\xi,\nu)=(1-\nu^2)\ln(1-\xi^2),\\&T_E(\xi,\nu)=(\xi^2-\nu^2)[\ln|s-\xi|-\ln(1-\xi^2)].\end{aligned} \tag{B44}$$

In performing the Hilbert transform (B43) we do not expect trouble from T_E, T_A, and T_B, but T_C and T_D are dangerous at $\xi\to\pm1$ where they become logarithmically divergent. However, the divergences arising from T_C and T_D cancel each other and the sum is finite. In order to handle this problem we introduce "safety" epsilons at the integration limits $\xi\to\pm1$, add the contributions from T_C and T_D, and finally pass to the limit of the epsilons tending to zero. In this way we obtain the following results for the different contributions to (B43):

$$G_{1A}(\nu)=-\tfrac{1}{4}\mathrm{P}\int_{-1}^{+1}d\xi\frac{T_A}{\xi-\nu}=-\tfrac{1}{4}(\nu^2-1)\ln\left|\frac{1-\nu}{1+\nu}\right|, \tag{B45}$$

$$\begin{aligned}G_{1B}(\nu)&=\tfrac{1}{4}(1-\nu^2)[(\ln|1-\nu|)^2-(\ln|1+\nu|)^2]+\frac{3\nu}{4}-\frac{\nu}{2}[(1-\nu)\ln|1-\nu|+(1+\nu)\ln|1+\nu|]\\&\quad-\tfrac{1}{8}[(1-\nu)^2\ln|1-\nu|-(1+\nu)^2\ln|1+\nu|],\end{aligned} \tag{B46}$$

$$G_{1E}(\nu)=-\tfrac{1}{4}(1-\nu^2)\ln\left|\frac{1-\nu}{1+\nu}\right|-\tfrac{1}{8}(1+\nu)^2\ln|1+\nu|+\tfrac{1}{8}(1-\nu)^2\ln|1-\nu|+\nu\ln2-\tfrac{3}{4}\nu, \tag{B47}$$

$$G_{1C}(\nu)+G_{1D}(\nu)=-\tfrac{1}{4}(1-\nu^2)\left((\ln|1-\nu|)^2-(\ln|1+\nu|)^2+\int_{(1+\nu)/(1-\nu)}^{(1-\nu)/(1+\nu)}\frac{dx}{x}\ln|1+x|\right). \tag{B48}$$

And finally,

$$\begin{aligned}G_1(\nu)&=G_{1A}(\nu)+G_{1B}(\nu)+G_{1C}(\nu)+G_{1D}(\nu)+G_{1E}(\nu)\\&=-\frac{1-\nu^2}{4}\int_{(1+\nu)/(1-\nu)}^{(1-\nu)/(1+\nu)}\frac{dx}{x}\ln|1+x|-\frac{\nu}{2}[(1-\nu)\ln|1-\nu|+(1+\nu)\ln|1+\nu|-2\ln2].\end{aligned} \tag{B49}$$

Note that $G_1(-\nu)=-G_1(\nu)$ so that it is only necessary to evaluate $G_1(\nu)$ for positive ν. To simplify the integral in (B49), introduce the function

$$g(a)=\begin{cases}\displaystyle\int_a^{1/a}\frac{dx}{x}\ln|1+x|, & \text{for } 0<a\leq1\\ -g(1/a), & \text{for } a\geq1.\end{cases} \tag{B50}$$

$g(a)$ is never needed at negative arguments since the θ functions in (B34) require that $|\nu|\leq1$ and hence that $(1-\nu)/(1+\nu)$ is always positive. It is easily seen that

$$g(a)=\tfrac{1}{2}(\ln a)^2+2\int_a^1\frac{dx}{x}\ln|1+x|. \tag{B51}$$

The function $g(a)$ can be evaluated numerically to very high precision since the integral occurring in it is well behaved and causes no problems. On using (B50) in (B49) we see that the expression for $G_1(\nu)$ goes over to that given in Eq. (2.15) of the text.

Evaluation of $G_2(x_1,x_2)$.

$$G_2(x_1,x_2)=-\tfrac{1}{4}\mathrm{P}\int_{-1}^{+1}d\xi\frac{T(\xi,x_1,x_2)}{\xi-x_1}, \tag{B52}$$

$$\begin{aligned}T(\xi,x_1,x_2)&=L(x_1^2+x_2,\xi,x_1)-L(x_1^2,\xi,x_1)\\&\quad-x_2\ln[A_1(\xi,x_1)].\end{aligned} \tag{B53}$$

On using (B38) to evaluate the right-hand side of the above expression we end up exactly with Eq. (2.23) of the text. Equation (B52) is now reduced to a principal value integral which has to be evaluated numerically. A detailed examination of Eq.

(2.23) for T shows that it is well behaved and finite everywhere except on the line $\xi = \nu + k$, where it is logarithmically divergent. Nevertheless, the integral (B52) is finite and thus as long as the integration knots are chosen off the line $\xi = \nu + k$, there is no problem with numerical work and G_2 can be computed to good accuracy.

APPENDIX C: NUMERICAL REPRESENTATION

Function $S(k)$ is expressed in terms of another function $F(x)$ defined by

$$S(k) = 1 - (1-x)^2 F(x), \tag{C1}$$

where

$$x = k^2/(k_0^2 + k^2) \tag{C2}$$

with a parameter k_0 chosen from the range $[1, 1.5]$.

By introducing a new variable x (C2), an infinite range of k is reduced to $[0,1]$ range of x. The definition (C1) of $F(x)$ allows us easily to satisfy the small-k (7.5) and large-k (7.6) asymptotic properties of $S(k)$. They lead to the following restrictions on $F(x)$:

$$F(0) = 1, \tag{C3}$$

$$F'(0) = 2 - k_0^2/2\omega_p, \tag{C4}$$

$$F(1) = -C/k_0^4. \tag{C5}$$

Function $F(x)$ is approximated by a cubic spline on the range $[0,1]$, whose coefficients are fitted by means of least squares to the set of $(k_i, S(k_i))$ points, with boundary conditions (C3)–(C5). Generated in this way the numerical procedure allows us to obtain an interpolated value of $S(k)$ at arbitrary k, as a continuous and smooth function.

---

*On leave from the Institute of Nuclear Research, Swierk, 05-400 Otwock, Poland.

[1] D. Pines and D. Bohm, Phys. Rev. 85, 338 (1952); 92, 609 (1953).

[2] J. Lindhard, K. Dan. Vidensk. Selsk., Mat-fys. Medd. 28, 8 (1954).

[3] For a review of early work in the field see D. Pines and P. Nozières, *The Theory of Quantum Liquids* (Benjamin, Amsterdam, 1969).

[4] J. Hubbard, Proc. R. Soc. (London) A243, 336 (1957).

[5] K. S. Singwi, M. P. Tosi, R. H. Land, and A. Sjölander, Phys. Rev. 176, 589 (1968).

[6] D. J. W. Geldart and S. H. Vosko, Can. J. Phys. 44, 2137 (1966).

[7] L. Kleinman, Phys. Rev. 160, 585 (1967); 172, 383 (1968).

[8] D. C. Langreth, Phys. Rev. 181, 753 (1969); 187, 768 (1969).

[9] J. W. F. Woo and S. S. Jha, Phys. Rev. B 3, 87 (1971).

[10] A. K. Rajagopal, Phys. Rev. A 6, 1239 (1972).

[11] H. Yasuhara, J. Phys. Soc. Jpn. 36, 361 (1974).

[12] F. Toigo and T. O. Woodruff, Phys. Rev. B 2, 3958 (1970); 4, 371 (1971); 4, 4312 (1971).

[13] D. J. W. Geldart and R. Taylor, Can. J. Phys. 48, 155 (1970).

[14] D. J. W. Geldart and R. Taylor, Can. J. Phys. 48, 167 (1970).

[15] P. Vashishta and K. S. Singwi, Phys. Rev. B 6, 875 (1972).

[16] G. Niklasson, Phys. Rev. B 10, 3052 (1974).

[17] P. V. S. Rao, J. Phys. Chem. Solids 35, 669 (1974).

[18] A. A. Kugler, J. Stat. Phys. 8, 107 (1973); 12, 35 (1975).

[19] P. E. Batson, C. H. Chen, and J. Silcox, Phys. Rev. Lett. 37, 937 (1976); P. E. Batson, thesis, Mat. Sci. Center Report No. 2673, Cornell University, 1976.

[20] P. C. Gibbons, S. E. Schnatterly, J. J. Ritsko, and J. R. Fields, Phys. Rev. B 13, 2451 (1976).

[21] H. J. Hohberger, A. Otto, and E. Petrie, Solid State Commun. 16, 175 (1975).

[22] P. Zacharias, J. Phys. F 5, 645 (1975).

[23] P. M. Platzman and P. Eisenberger, Phys. Rev. Lett. 33, 152 (1974).

[24] P. K. Aravind, A. Holas, and K. S. Singwi (unpublished).

[25] See, for example, A. L. Fetter, and J. D. Walecka, *Quantum Theory of Many-Particle Systems* (McGraw-Hill, New York), Sec. 12.

[26] See Ref. 25, p. 174.

[27] See the discussion in Ref. 3, p. 104.

[28] K. N. Pathak and P. Vashishta, Phys. Rev. B 7, 4300 (1973).

[29] D. F. DuBois, Ann. Phys. (N.Y.) 8, 24 (1959).

[30] P. Nozières and D. Pines, Phys. Rev. 111, 442 (1958).

[31] A. J. Glick, Phys. Rev. 129, 1399 (1963).

[32] M. Gell-Mann and K. A. Brueckner, Phys. Rev. 106, 181 (1957).

[33] F. Brosens, L. F. Lemmens, and J. T. Devreese, Phys. Status Solidi B 74, 45 (1976); 80, 99 (1977).

[34] M. W. C. Dharma-wardana, J. Phys. C 9, 1919 (1976).

[35] D. N. Tripathy and S. S. Mandal, Phys. Rev. B 16, 231 (1977).

[36] S. S. Mandal, B. K. Rao, and D. N. Tripathy, Phys. Rev. B 18, 2524 (1978).

[37] D. N. Tripathy, B. K. Rao, and S. S. Mandal, Solid State Commun. 22, 83 (1977).

[38] In a recent publication dealing with the first-order perturbation theory as applied to the two-dimensional electron gas [P. F. Maldugue, Solid State Commun. 26, 133 (1978)], an analogous peaked structure in Q^1 is found at $k \approx 2$. Since it originates from the repeated propagators G_0 occuring in Q^1 rather than in the long-range character of the interaction, as we have shown in the three-dimensional case, it is insensitive to the details of the screening of the interaction. From this we conclude, in contrast to the author, that the occurrence of the peak is not a genuine effect, but an artifact of the first-order perturbation theory.

[39] B. K. Rao, S. S. Mandal, and D. N. Tripathy, J. Phys. F (to be published).

[40]J. T. Devreese, F. Brosens, and L. F. Lemmens, Phys. Status Solidi B 91, 349 (1979).
[41]D. N. Tripathy, S. S. Mandal, and B. K. Rao, Phys. Status Solidi B (to be published).
[42]J. C. Kimball, Phys. Rev. A 7, 1648 (1973).
[43]F. Brosens, L. F. Lemmens, and J. T. Devreese, Phys. Status Solidi B 82, 117 (1977).
[44]J. C. Kimball, Phys. Rev. B 14, 2371 (1976).
[45]H. B. Singh and K. N. Pathak, Phys. Rev. B 10, 2764 (1974) (in their formula, corresponding to our (3.4), there is an error in the constant term).
[46]F. Brosens, L. F. Lemmens, and J. T. Devreese, Phys. Status Solidi B 81, 551 (1977).